Remote Sensing of Environment 344 (2026) 115534

Contents lists available at ScienceDirect

Remote Sensing of Environment

journal homepage: www.elsevier.com/locate/rse

An independent evaluation of global 1 km soil moisture products using in-situ and airborne observations

Yilin Ma [a,b], Liujun Zhu [a,c,*], Shanshui Yuan [a], Junliang Jin [a], Zhengyang Tang [d], Jeffrey P. Walker [c]

[a] State Key Laboratory of Water Disaster Prevention, Yangtze Institute for Conservation and Development, Hohai University, Nanjing 210098, China
[b] College of Geography and Remote sensing, Hohai University, Nanjing 210098, China
[c] Department of Civil and Environmental Engineering, Monash University, Clayton, Vic 3800, Australia
[d] China Yangtze Power Co., Ltd. (CYPC), Wuhan Hubei 430000, China

ARTICLE INFO

Editor: Jing M. Chen

Keywords:
Soil moisture evaluation
Soil moisture products
High resolution
Field experiments

ABSTRACT

High-resolution soil moisture data are essential for applications in agriculture, hydrology, and disaster management. Four global daily SM products at 1 km resolution have recently been developed, being the Seamless Soil Moisture (SSM), Global Surface Soil Moisture (GSSM), Global Land Surface Satellite (GLASS), and a downscaled SMAP product (DSMAP). These products rely on either machine learning or empirical regression models, offering significant potential but raising concerns regarding their generalization capability and spatial fidelity. Previous evaluations of these high-resolution products have relied predominantly on point-scale comparisons using the same in-situ networks employed for model training. Consequently, this study provides an independent evaluation using 1545 global in-situ stations excluded from product development and airborne passive microwave measurements from five field campaigns across North America and Australia. Results reveal that none of the evaluated products met the target unbiased Root Mean Square Error (ubRMSE) of 0.04–0.06 m^3/m^3, with observed values ranging from 0.097 to 0.104 m^3/m^3. All products exhibited narrower dynamic ranges (0.10–0.30 m^3/m^3) than those of in-situ observations (0.05–0.40 m^3/m^3), particularly underestimating wet and overestimating dry extremes. GLASS ($R = 0.576$) and DSMAP ($R = 0.556$) generally outperformed GSSM ($R = 0.504$) and SSM ($R = 0.399$) in capturing temporal dynamics relative to ground measurements. Spatially, airborne-based evaluation highlighted limitations in capturing fine-scale heterogeneity, particularly for SSM (mean $R = 0.19$) and GSSM (mean $R = 0.31$), which showed a narrow dynamic range and nearly static spatial pattern with weak response to regional rainfall. In contrast, DSMAP effectively captured the temporal dynamics of airborne data (mean $R = 0.57$) but retained coarse resolution artifacts from its downscaling process. Expanding training datasets, enhancing the generalization capability of the machine learning methods employed, and conducting rigorous spatial evaluations are identified as critical steps to ensure the reliability of high-resolution soil moisture products for operational applications.

1. Introduction

Soil moisture plays a pivotal role in the terrestrial hydrological cycle, influencing land–atmosphere energy exchanges, vegetation dynamics, and the distribution of precipitation between infiltration and runoff (Legates et al., 2011). Reliable soil moisture information is essential for various applications, including irrigation scheduling, drought and flood forecasting, and climate modeling (Chen et al., 2017). However, acquiring high-quality soil moisture data at appropriate spatiotemporal resolutions remains challenging, particularly at continental scale (Colliander et al., 2017a; Petropoulos et al., 2015). In-situ soil moisture measurements provide high accuracy but are limited in spatial coverage, especially in remote or data-scarce regions. In recent decades, remote sensing technologies have become widely used for large-scale near-surface soil moisture monitoring (Babaeian et al., 2021). This study focuses on the near-surface soil moisture within the top 0–5 cm, which is

* Corresponding author at: State Key Laboratory of Water Disaster Prevention, Yangtze Institute for Conservation and Development, Hohai University, Nanjing 210098, China.
E-mail addresses: Liujun.zhu@hhu.edu.cn, Liujun.zhu@Monash.edu (L. Zhu).

https://doi.org/10.1016/j.rse.2026.115534
Received 28 October 2025; Received in revised form 30 April 2026; Accepted 7 June 2026
Available online 12 June 2026

critical for characterizing land-atmosphere interactions and is the primary target of L-band microwave remote sensing.

There are currently two passive microwave satellite missions dedicated to soil moisture observation, being the Soil Moisture Active Passive (SMAP) (Entekhabi et al., 2010) and Soil Moisture and Ocean Salinity (SMOS) (Kerr et al., 2010). While these missions have achieved significant success in global soil moisture mapping, their coarse native spatial resolutions (36 km for SMAP and 43 km for SMOS) limit their ability to capture fine-scale variability and thus their usefulness in applications that require high spatial detail. Many studies have shown that soil moisture data at finer spatial resolutions, around 1 km, can be used to significantly enhance the accuracy of hydrological and climatic process modeling (Merlin et al., 2006a; Merlin et al., 2006b). High-resolution soil moisture data also supports practical applications that rely on detailed spatial variability. For example, it enables field-level irrigation management in precision agriculture, improves the detection of localized flood and drought risks, enhances landslide forecasting by capturing slope-specific moisture conditions, and strengthens wildfire risk assessment by identifying dry zones with greater precision (Dandridge et al., 2020; Fan et al., 2025; Peng et al., 2021).

Various downscaling methods have been proposed to achieve higher spatial resolution (Peng et al., 2017; Senanayake et al., 2024). Despite these efforts, generating reliable soil moisture estimates at resolutions of 1 km or finer remains a considerable challenge (Sabaghy et al., 2018). Synthetic Aperture Radar (SAR) has the capability to directly provide high-resolution soil moisture estimates (Zhu et al., 2022; Zhu et al., 2023). However, its application at the global scale remains challenging due to limited temporal coverage, signal interference from vegetation and surface roughness, the complexity involved in data preprocessing, and the difficulty in calibrating retrieval methods across diverse landscapes (Rahmati et al., 2026). Optical and thermal infrared remote sensing technologies also have high spatial resolutions, with many successful applications in soil moisture estimation presented in literature (Chauhan et al., 2003; Zhang and Zhou 2016b). However, their effectiveness is often limited by cloud cover, atmospheric interference, and the indirect nature of the retrieval, making them less reliable for consistent, large-scale soil moisture monitoring (Zhang and Zhou 2016a).

Despite these challenges, four global-scale soil moisture products with daily temporal resolution and approximately 1-km spatial resolution have been recently developed, offering promising solutions for fine-scale hydrological and environmental applications. Zheng et al. (2023) developed the Seamless Soil Moisture (SSM) product by applying a Random Forest algorithm to disaggregate coarse-resolution satellite data into 1 km resolution, using multi-source optical remote sensing inputs and in-situ measurements from the International Soil Moisture Network (ISMN, Dorigo et al., 2021). Han et al. (2023) produced the Global Surface Soil Moisture (GSSM) product, which integrates satellite observations, the fifth generation European Centre for Medium-Range Weather Forecasts (ECMWF) atmospheric reanalysis (ERA5-land) data, and ISMN measurements. This was achieved through a Random Forest model that utilizes input predictors that are physically relevant to soil moisture dynamics, thereby enhancing both the physical consistency and the overall predictive accuracy. Zhang et al. (2023) produced the Global Land Surface Satellite (GLASS) SM product using an eXtreme Gradient Boosting (XGBoost) model, combining GLASS remote sensing products, ERA5-Land data, ISMN observations, and static auxiliary variables in an ensemble learning framework to improve robustness and spatial detail. Fang et al. (2022) proposed a thermal inertia-based downscaling algorithm to refine 9 km SMAP data to 1 km resolution. By establishing an inverse relationship between land surface temperature and soil moisture, and stratifying the model by Normalized Difference Vegetation Index (NDVI) levels, the sensitivity to vegetation dynamics and surface heterogeneity was improved.

Unlike traditional retrieval algorithms based on radiative transfer or scattering models, the three seamless daily products (SSM, GSSM and GLASS) were developed using machine learning techniques, which enable flexible integration of multi-source data and an improved adaptability across diverse environmental conditions. However, it is widely acknowledged that the performance of machine learning models strongly depends on the availability and quality of training samples (Zhu et al., 2025b), particularly the accuracy, spatial representativeness, and temporal coverage of ground truth data. Although global in-situ soil moisture measurements from the ISMN were partly used in the development of these products, the uneven spatial distribution of ISMN stations raises concerns about model performance in regions lacking training data. Furthermore, all of the studies randomly divided in-situ measurements into training and testing sets, which may introduce dependencies between the two subsets. This practice can compromise model stability and accuracy, potentially leading to overfitting (Liu, 2023; Ramo et al., 2018). In addition, spatial evaluation remains an essential yet often overlooked aspect in the accuracy assessment of high-resolution soil moisture products, as the spatial distribution of soil moisture plays a critical role in regulating runoff generation, evapotranspiration, and land–atmosphere interactions (Lakhankar et al., 2010). Point-scale evaluation approaches are insufficient for evaluating the spatial patterns of soil moisture, especially in areas with sparse ground observations and complex surface heterogeneity. The spatial mismatch between in-situ measurements and satellite-derived soil moisture products further complicates the assessment of dynamic soil moisture variations. Such limitations in evaluation strategies and the uncertainty in accuracy assessment greatly restrict broader application and reliability of these high-resolution soil moisture products, particularly in regions with limited ground observations or complex land surface conditions.

In this study, the four global daily soil moisture products at 1-km resolution were independently evaluated to support enhanced applications. A more comprehensive ground truth dataset was constructed by integrating in-situ measurements from the ISMN along with data from several additional monitoring networks. This dataset was used to perform an independent evaluation of each product, aiming to reduce bias introduced by training data overlap. Moreover, high-resolution soil moisture data from three series of airborne campaigns conducted across North America and Australia were used for comparative analysis, allowing the first spatially explicit evaluation of these soil moisture products. The evaluation was designed to (1) assess real-world performance of the four products beyond official validation reports, particularly given their reliance on machine learning or empirical regression relationships; (2) examine the spatial patterns captured by each product using airborne estimates, offering insights into their ability to capture fine-scale spatial distributions and dynamic variability; and (3) provide practical guidance for end users and inform future development of high-resolution soil moisture datasets.

2. Data and methods

2.1. Soil moisture products

The SSM product is a secondary soil moisture product developed by Zheng et al. (2023), based on the European Space Agency-Climate Change Initiative (ESA-CCI) SSM product. To address data gaps in the original ESA-CCI product, an operational gap-filling procedure was applied using ERA5 data as auxiliary input. Subsequently, a random forest regression model was trained to downscale the coarse-resolution soil moisture data (0.25°) to a finer spatial resolution of 1 km. This disaggregation was based on the ISMN in-situ measurements, multi-source optical remote sensing datasets, and static terrain and soil texture variables. The resulting product (Version 1.0) provides global, seamless daily soil moisture estimates from 2000 to 2020 and is publicly accessible via the National Tibetan Plateau Science Data Center at https://data.tpdc.ac.cn/home (accessed 2024-03-15).

The GSSM product developed by Han et al. (2023) was generated

using a Random Forest model that integrates physically meaningful predictors, including meteorological forcing, static soil physical properties, and multi-source optical remote sensing data. A total of 18 predictors were selected to represent key atmospheric, land surface, and vegetation factors known to influence soil moisture dynamics, with temporal harmonization applied to ensure consistency across input sources. Similarly, this model was trained using in-situ measurements from the ISMN. The resulting product GSSM1.7 provides daily global near-surface soil moisture at a spatial resolution of 1 km for the period from 2000 to 2020. The dataset is publicly available at https://github.com/QianqianHan96/GSSM1km (accessed 2024-03-07).

The GLASS soil moisture product (version 1.0) is a spatiotemporally continuous, global daily dataset at 1 km resolution for the period from 2000 to 2020. This product was generated using an XGBoost model from other GLASS datasets, ERA5-Land reanalysis data, auxiliary environmental datasets, and ground-based soil moisture observations from the ISMN (Zhang et al., 2023). The dataset is publicly available at http://glass.umd.edu/soil_moisture/ (accessed 2024-02-19).

Fang et al. (2022) developed a soil moisture downscaling model based on thermal inertia theory to disaggregate the SMAP Enhanced L2 radiometer 9 km product to a 1 km resolution. For simplicity, this product is referred to as DSMAP throughout this study. The algorithm relies on an empirical linear relationship between soil moisture and diurnal land-surface-temperature (LST) variations, stratified by NDVI groups to account for vegetation conditions. Because this relationship is derived from regression fitting using the Global Land Data Assimilation System Noah land surface (GLDAS-Noah) model outputs, the resulting 1 km estimates are fundamentally empirical and therefore require independent validation against in-situ measurements. DSMAP is provided at the SMAP descending (06:00 AM) and ascending (06:00 PM) overpass times. As the descending overpass is generally considered more reliable, only the descending data were evaluated in this study. Although the product is nominally daily, spatial gaps caused by missing SMAP enhanced L2 radiometer half-orbit soil moisture product observations (SPL2SMP_E) were not filled, making it a quasi-daily dataset. This product (version 1) spans from April 1, 2015 to September 29, 2022, and is freely available from the National Snow and Ice Data Center (NSIDC) at https://nsidc.org/data/nsidc-0779/versions/1 (accessed 2024-02-23).

2.2. In-situ datasets

The in-situ soil moisture observations used in this study were obtained from a range of global ground-based monitoring networks. The primary data source was the International Soil Moisture Network (ISMN; https://ismn.geo.tuwien.ac.at/), providing harmonized and quality-controlled SM data, and serving as a valuable resource for the evaluation and development of satellite- and model-based soil moisture products. As of July 2021, the ISMN had integrated measurements from 71 operational networks and more than 2800 stations worldwide (Dorigo et al., 2021), and continues to expand.

In addition to the ISMN, supplementary in-situ data were collected from several regional and national networks that had not been incorporated into the ISMN at the time of this study. This expansion was necessary because most of the ISMN stations had already been used in the development of the four SM products. The additional data sources included several soil moisture observation networks in China covering the 2000–2020 period. These consisted of stations from Tibet-Obs that were unavailable through the ISMN, SONTE-China observations recorded before 2020 (Wang et al., 2023), QLB-NET (Chai et al., 2024), and the Genhe and Saihanba observation networks (Jiang et al., 2020). These networks collectively provide detailed measurements across diverse ecological zones, enhancing spatial representativeness. In southeastern Australia, several OzNet stations not included in the ISMN were also used (Smith et al., 2012), while in the United States, data from the Little Washita and Fort Cobb watershed networks were incorporated (Yang et al., 2020). Additionally, the Raam network in the Netherlands was included in the evaluation (Benninga et al., 2018).

2.3. Auxiliary data

Landcover, climate zone and soil texture datasets were used to assess the performance of soil moisture products under varying environmental conditions. These variables represent the most fundamental and widely recognized factors on surface soil moisture dynamics and are consistently available at global scales, allowing for a fair comparison across the four soil moisture products evaluated in this study. Landcover information was derived from the 2023 MODIS MCD12C1 product at a spatial resolution of 0.05°. The original 17 categories of International Geosphere-Biosphere Programme (IGBP) classification scheme were reclassified into four generalized types including cropland, forest, grassland, and others to ensure a sufficient number of stations for evaluation. The “others” category includes barren land, urban and built-up areas, and wetland or snow. While some of these categories and water bodies are commonly masked in many soil moisture products, they were retained here because a 1 km grid cell may be classified as part of the “others” category even though the ground station is situated on valid soil. Furthermore, since the four evaluated products did not mask these categories in their original releases, they were included to ensure that the evaluation reflects the actual performance of the data as provided for operational use.

Climate zones following the Köppen–Geiger system were reorganized into four primary classes including tropical (A), arid (B), temperate (C), and cold and polar (D and E) (Peel et al., 2007; Rubel and Kottek, 2010). Soil texture information was extracted from the Harmonized World Soil Database (HWSD) version 2.0. This database provides global soil property data at 30 arc-seconds (IIASA, F, 2023), which closely corresponds to the 1 km resolution of the four evaluated products. To ensure a sufficient number of stations for evaluation within each category, the soil texture classes were reclassified into four types, consisting of clay, loam, sandy loam, and sand.

2.4. Airborne datasets

Five airborne soil moisture campaigns conducted between 2012 and 2016 specifically for calibration and evaluation of the SMAP concept were included in this study (Table 1). These campaigns were categorized into two series based on their geographic locations. The native spatial resolution of these airborne estimates ranged from 0.5 to 1.5 km (Table 1) and so were resampled to 1 km using cubic convolution interpolation to match the soil moisture products being evaluated. The first series is the SMAP Evaluation Experiments that were made across North America, including the SMAPVEX12, SMAPVEX15 and SMAPVEX16. A few early campaigns, e.g. SMAPVEX08 (Park et al., 2011), were not included as >90% of its pixels were labeled as no data. The Passive and Active L and S Band Microwave Instrument (PALS) was the main sensor used in these North American campaigns (Colliander et al., 2012), and so the derived near-surface soil moisture from PALS were used for intercomparison in this study.

The SMAPVEX12 campaign was made from June 7 to July 19, 2012, over an agricultural region in southern Manitoba, Canada. PALS flights were conducted at a 1500 m spatial resolution, with soil moisture retrievals in non-forested areas showing strong agreement with ground measurements (R = 0.87, RMSE = 0.058 m^3/m^3) (Colliander et al., 2016). The SMAPVEX15 campaign was made in southeastern Arizona, USA from August 2 to 18, 2015, with PALS observations acquired at a 500 m spatial resolution. The retrieved soil moisture values achieved an R and RMSE of 0.83 and 0.016 m^3/m^3 (Colliander et al., 2017a).

The SMAPVEX16 experiment was conducted over two regions, being the SMAPVEX16-IA in Iowa, USA, and the SMAPVEX16-MB in Manitoba, Canada. SMAPVEX16-IA was undertaken in two separate periods, being May 28 to June 5 and August 3 to 16, 2016 in order to achieve

Table 1
Description of each field campaign utilized in the evaluation process.

Name	Location	Flight area	Spatial resolution [m]	Flight	Date	Main Landcover	Köppen Climate Type
SMAPVEX12	Canada	Manitoba	1500	15	June 7–July 19, 2012	Cropland and Forest	Dfb
SMAPVEX15	US	Arizona	1500	7	August 2–18, 2015	Shrubland and Grassland	BSh
SMAPVEX16	US	Iowa	500	12	May 28–June 5 and August 3–16, 2016	Cropland	Dfa
	Canada	Manitoba	500	12	June 8–20 and July 10–22, 2016	Cropland and Forest	Dfb
SMAPEx-4	Australia	Yanco	1000	8	May 1–22, 2015	Grassland and Cropland	Cfa
SMAPEx-5	Australia	Yanco	1000	8	September 7–27, 2015	Grassland and Cropland	Cfa

Table 2
List of independent evaluation set utilized in this study. Grid cells with a similar area ratio ≥ 0.82 were classified as core cells, while the remaining stations were designated as extra cells.

Product	Core grid cells		Extra grid cells	
	# grid cells	# stations	# grid cells	# stations
SSM	184	290	228	298
GSSM	182	352	213	274
GLASS	679	1241	773	897
DSMAP	544	760	903	1008

different vegetation and soil moisture conditions (Colliander et al., 2017c). SMAPVEX16-MB was conducted from June 8 to 20 and July 10 to 22, 2016, covering the same location as SMAPVEX12, but with a slightly different spatial extent. Both regions were observed using PALS at a 500 m spatial resolution. The retrieved soil moisture data demonstrated high accuracy, with RMSE values below 0.04 m^3/m^3 and R values exceeding 0.85 (Colliander et al., 2019).

The second series of airborne campaigns include the Soil Moisture Active Passive Experiments 4 and 5 (SMAPEx-4 and SMAPEx-5). They were made in the Yanco agricultural area of southeastern Australia. These campaigns provided a unique opportunity for evaluating and calibrating the SMAP active/passive soil moisture retrieval concept in the Southern Hemisphere and include the only experiment to be undertaken while the SMAP radar was still operational. SMAPEx-4 was carried out during the Australian autumn (May 1–22, 2015), and SMAPEx-5 during the summer (September 7–27, 2015), with each campaign comprising eight flights. Observations were collected using the Polarimetric L-band Multi-beam Radiometer (PLMR), which provided soil moisture estimates at a spatial resolution of approximately 1 km. The PLMR-retrieved soil moisture showed strong agreement with in-situ measurements, achieving RMSE values of 0.05–0.07 m^3/m^3 for SMAPEx-4 and 0.05–0.09 m^3/m^3 for SMAPEx-5, after excluding pixels

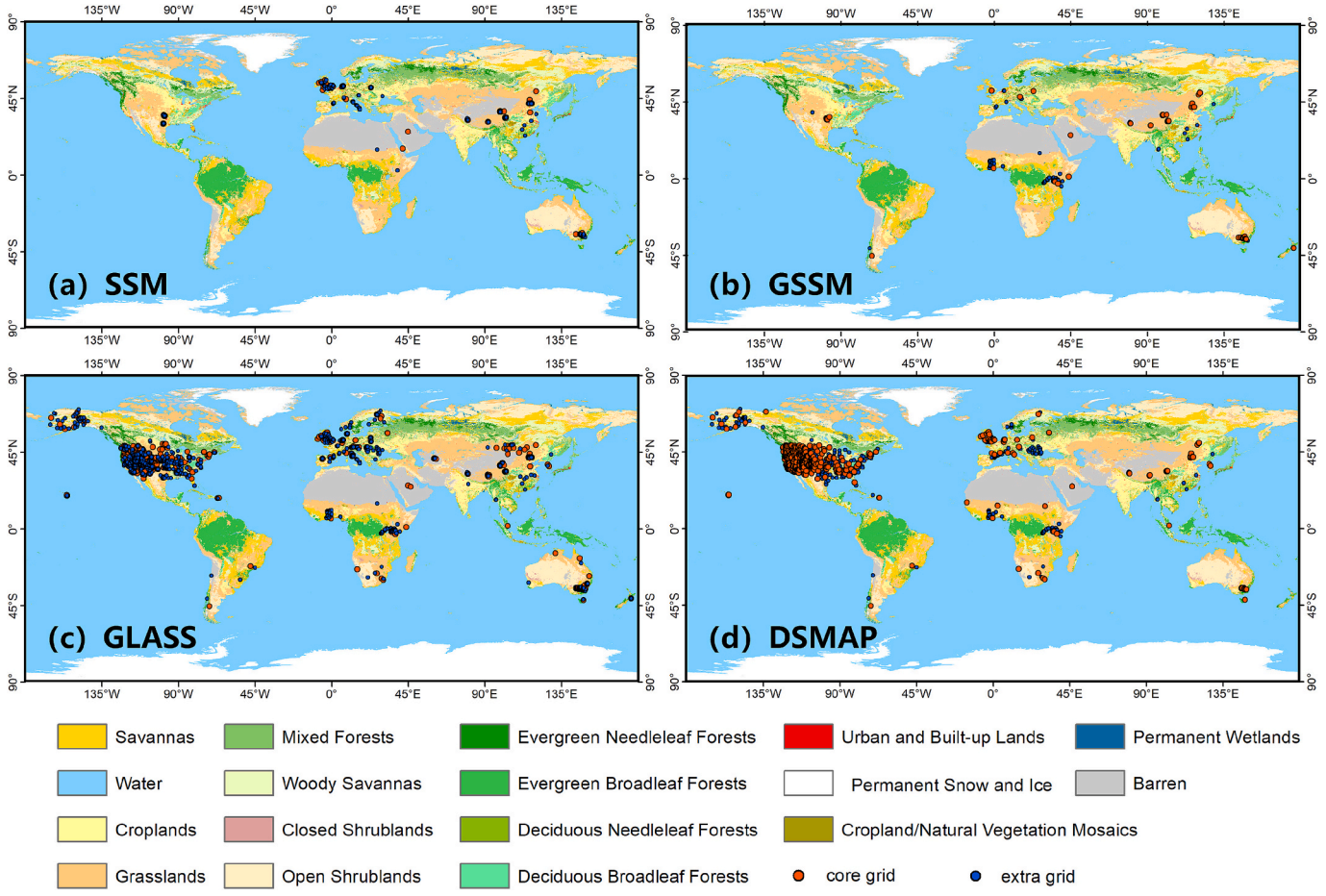

Fig. 1. Global distribution of the core and extra grid cells for (a) SSM, (b) GSSM, (c) GLASS and (d) DSMAP. Grid cell locations are overlaid on the MODIS IGBP landcover map, with colors indicating the corresponding global landcover classes. Grid cells with a similar area ratio ≥ 0.82 were classified as core cells, while the remaining stations were designated as extra cells.

affected by standing water (Ye et al., 2021).

2.5. Evaluation methods

A comprehensive evaluation of four downscaled soil moisture products was conducted in this study using both long-term point-based in-situ soil moisture measurements and short-term spatially intensive airborne passive microwave derived soil moisture estimates. The in-situ soil moisture data for the top 5 cm soil layer were collected from a range of global monitoring networks covering the period from 2000 to 2020. To ensure the independence and fairness of the evaluation, only in-situ measurements that were not used in the development, calibration or evaluation of the four soil moisture products were used. Specifically, all stations with site names identical to those reported as training, calibration or evaluation stations were filtered out. This enabled an unbiased assessment of product performance across diverse environmental conditions, with the spatial distribution of these independent evaluation sites illustrated in Fig. 1. It should also be noted that many more stations were used in the production of the SSM and GSSM products than for GLASS and DSMAP. DSMAP has the largest number of stations as the in-situ measurements were not directly used in the development of model.

Two ground-truth datasets were prepared for the four evaluated products. To match the daily resolution of the GSSM, GLASS, and SSM products, in-situ measurements were averaged by date. For DSMAP, only observations collected between 05:00 and 07:00 local time were used as the reference, consistent with the SMAP descending overpass. For each 1 km grid cell, the mean of all stations located within that cell was calculated to represent the 0–5 cm reference soil moisture, which is comparable to the sensing depth of the airborne L-band passive measurements (Ye et al., 2021).

Grid cells were categorized into core and extra grid cells based on the similar area ratio of sites (LC-area, Peng et al., 2025). This metric is defined as the ratio of number of sub-grid cells within a grid cell that share the same landcover type as the ground station to the total number of sub-grid cells in that grid cell. High-resolution landcover data from the 10 m ESA WorldCover dataset were used to calculate this consistency. A higher LC-area indicates that the station's local environment is more characteristic of the entire grid cell, thereby reducing spatial representativeness errors caused by sub-grid environmental heterogeneity. Following the threshold derived by Peng et al. (2025), grid cells with an LC-area ≥ 0.82 were classified as core cells, while the remaining stations were designated as extra cells. Although this threshold was originally developed for coarse-resolution products (tens of kilometers), its application in this study is considered conservative because the spatial mismatch between point-scale measurements and 1 km grid cells is substantially smaller. Therefore, if a station located within the dominant land-cover type can be regarded as representative of a much larger grid cell when the dominant class exceeds 82% of the area, the same criterion is expected to be at least as valid for 1 km grid cells. In this study, the threshold is thus adopted as a literature-based and physically reasonable criterion to ensure station representativeness, rather than an optimized value specific to the dataset. Moreover, a sensitivity analysis was conducted (Fig. A1) by varying the LC-area threshold from 0.70 to 0.85 at intervals of 0.05. The results indicate that the evaluation outcomes are generally insensitive to the choice of threshold. Specifically, the RMSE of each product varies by no more than 0.015 m^3/m^3, while the R values of most products change by less than 0.05. Although GSSM exhibits the largest variation in R (0.16), its RMSE remains nearly stable (0.099–0.105 m^3/m^3), suggesting that the influence of this parameter is marginal within a reasonable range.

Four widely used accuracy metrics were employed, being the Pearson correlation coefficient (R), Bias, Root Mean Square Error (RMSE), and Unbiased Root Mean Square Error (ubRMSE). These metrics are defined as

$$R = \frac{\sum_{i=1}^{n}\left(SM_{p,i} - \overline{SM_p}\right)\left(SM_{o,i} - \overline{SM_o}\right)}{\sqrt{\sum_{i=1}^{n}\left(SM_{p,i} - \overline{SM_p}\right)^2}\sqrt{\sum_{i=1}^{n}\left(SM_{o,i} - \overline{SM_o}\right)^2}} \quad (1)$$

$$\text{Bias} = \frac{1}{n}\sum_{i=1}^{n}\left(SM_{p,i} - SM_{o,i}\right) \quad (2)$$

$$\text{RMSE} = \sqrt{\frac{1}{n}\sum_{i=1}^{n}\left(SM_{p,i} - SM_{o,i}\right)^2} \quad (3)$$

$$\text{ubRMSE} = \sqrt{\text{RMSE}^2 - \text{Bias}^2}, \quad (4)$$

Where SM_p represents the soil moisture value from each of the four satellite products and SM_o denotes the reference observations. The overbar indicates the average of n samples. For the ground-based evaluation, SM_o refers to the in-situ measurement while for the airborne-based evaluation, SM_o refers to the airborne passive microwave estimates. Because airborne estimates were considered approximations of the ground truth rather than absolute truth, the terms RMSE and ubRMSE in Eq. 3 and 4 are referred to as Root Mean Square Difference (RMSD) and Unbiased Root Mean Square Difference (ubRMSD) in that context, respectively.

The accuracy of soil moisture products varies substantially across different environmental conditions (Al-Yaari et al., 2019; Meng et al., 2024a). In this study, product performance was evaluated across diverse landcover, climate, and soil-texture scenarios. As described in Section 2.3, each environmental variable was grouped into four categories, allowing a larger number of grid cells to be included in each class and thereby improving the statistical robustness of the results. The number of available grid cells in each category is provided in Table A2 in the Appendix.

Airborne passive microwave soil moisture estimates were used as reference data to approximate ground truth. The GSSM, GLASS and SSM are provided in Coordinated Universal Time (UTC), while the airborne measurements, originally recorded in local time during the flight campaigns, were converted to UTC based on the corresponding flight dates and geographic locations. Temporal alignment was subsequently performed by selecting, for each product date, the nearest airborne observation in time. For the DSMAP, the airborne campaigns used in this study were specifically designed for SMAP validation and thus provide well-matched soil moisture estimation. As a result, potential sub-daily soil moisture response lags associated with precipitation and infiltration processes are expected to have limited influence on the comparison results. In addition to visual comparisons of spatial patterns, quantitative spatial evaluation was conducted using the same accuracy metrics described earlier.

3. Evaluation using ground soil moisture

3.1. Overall performance

Fig. 2 presents the evaluation results of the four soil moisture products against in-situ observations from the core grid cells. Among the four products, GLASS generally performed best, achieving the highest correlation (0.576) and low RMSE (0.105 m^3/m^3) and ubRMSE (0.097 m^3/m^3). However, a relatively large bias of −0.041 m^3/m^3 was observed. This bias primarily originated from the underestimation at mid to high soil moisture values (>0.25 m^3/m^3; Fig. 2e), whereas the scatter points at low values (< 0.15 m^3/m^3) were largely aligned with the 1:1 line (Fig. 2c). This behavior differs from many existing machine-learning-based studies (Mao et al., 2022), as well as from the patterns of SSM and GSSM (Fig. 2a and b), where low values tend to be substantially overestimated and high values underestimated due to the learning

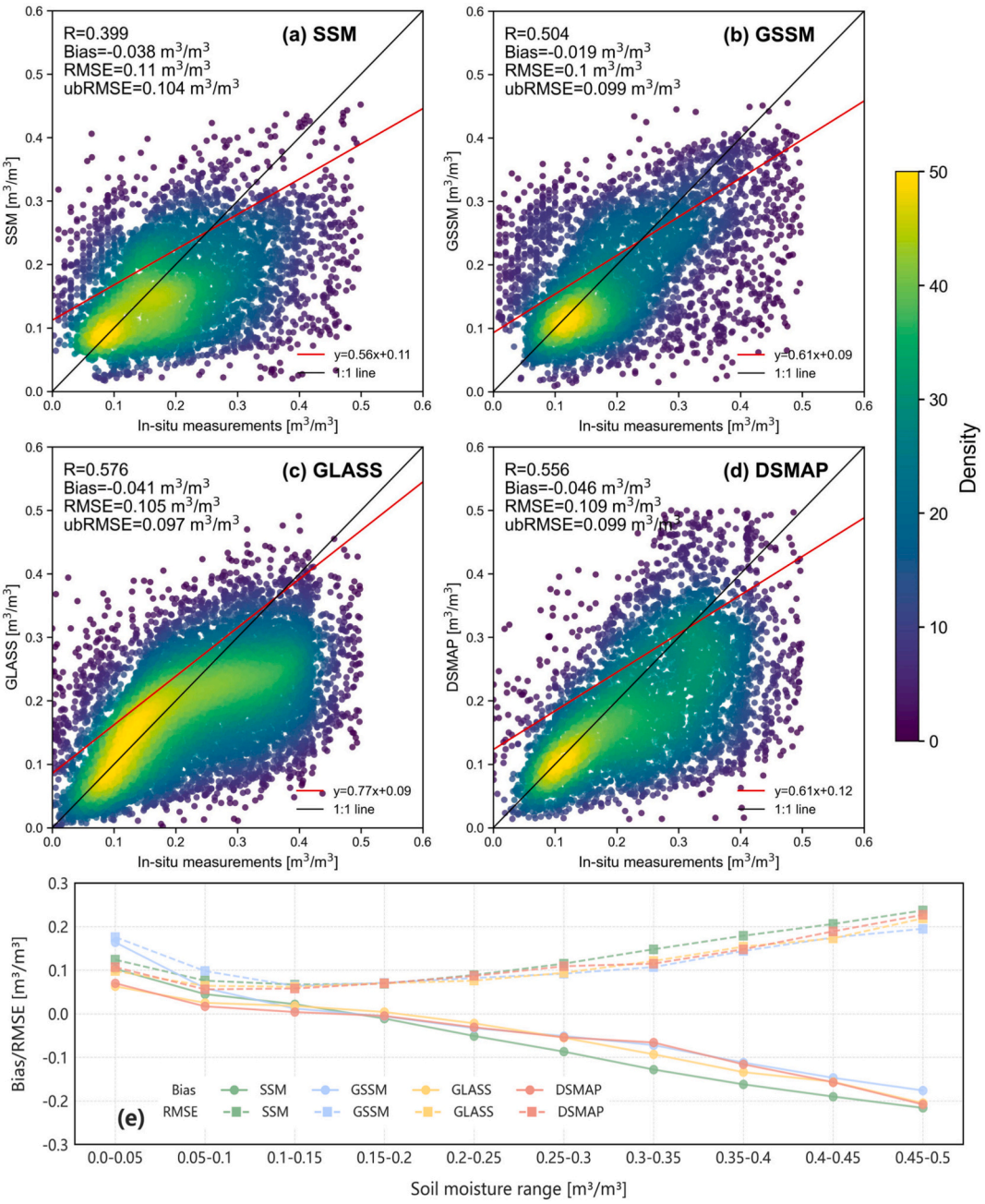

Fig. 2. Scatterplots comparing the four soil moisture products with in-situ measurements across the core grid cells. (a)–(d) show the results for SSM, GSSM, GLASS, and DSMAP, respectively. (e) presents the range-specific bias and RMSE for the four products.

process gravitating toward the global mean to reduce training loss.

The relatively strong performance of GLASS is likely attributable to the implementation of Triple Collocation (TC, McColl et al., 2014) to identify representative training stations for the XGBoost model. DSMAP also showed strong agreement with the in-situ measurements, with a slightly lower correlation (0.556) and slightly larger bias (-0.046 m^3/m^3) and RMSE (0.109 m^3/m^3). Similar to GLASS, the relatively large bias primarily resulted from the underestimation of high soil moisture values. GSSM demonstrated comparable performance, characterized by a moderate correlation (0.504), the smallest bias (0.019 m^3/m^3), and relatively low RMSE (0.100 m^3/m^3) and ubRMSE (0.099 m^3/m^3). However, the minimal overall bias reported for GSSM is largely attributable to the substantial positive bias at low soil moisture levels, which offsets the negative bias observed at higher levels. In contrast, SSM showed more moderate performance, with the lowest correlation (0.399), a notable negative bias (-0.038 m^3/m^3), and the largest RMSE (0.110 m^3/m^3). Both GSSM and SSM failed to capture dry extremes (Fig. 2e), with the minimum SSM values clustering around 0.02 m^3/m^3.

Fig. 3 presents the boxplots of the accuracy metrics estimated for each grid cell, including the core grids, the extra grids, and their combination. GSSM and GLASS achieved significantly higher ($p < 0.05$, Student's t-test) median correlations than DSMAP (median $R = 0.439$) and SSM (median $R = 0.383$). This pattern differs from the overall results in Fig. 2, where the aggregated correlation of DSMAP matched or exceeded that of GSSM and GLASS. SSM achieved the smallest interquartile range of R, followed by GSSM, DSMAP and GLASS.

GSSM, GLASS, and DSMAP achieved nearly identical median RMSE values (0.087–0.088 m^3/m^3), which were substantially lower than their corresponding overall RMSEs (0.100–0.109 m^3/m^3). Among these three products, GSSM exhibited the fewest high-RMSE outliers and the

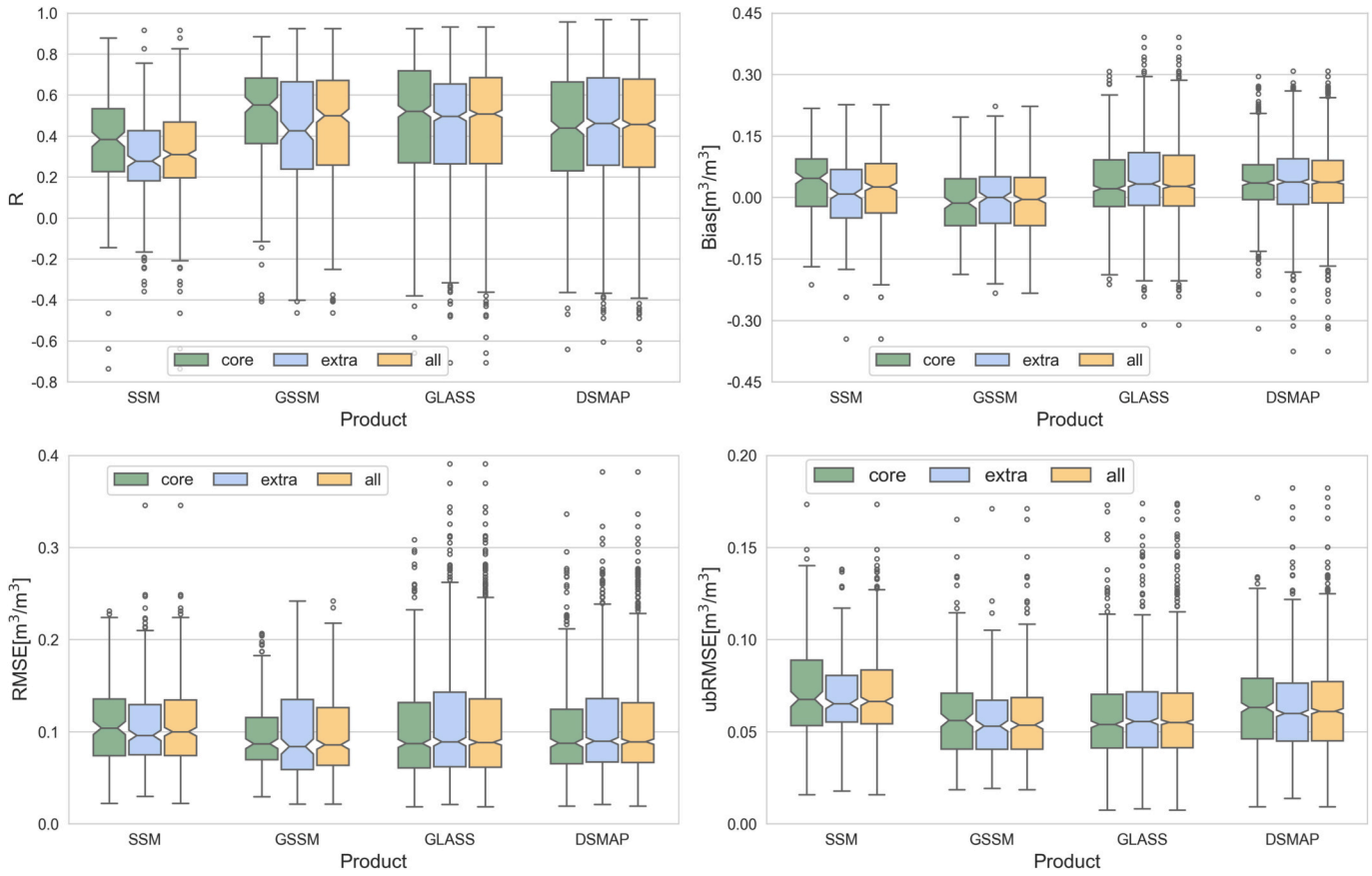

Fig. 3. Boxplots of grid specific performance on core, extra and all grid cells. The number of available grid cells for each type is listed in Table 2.

smallest interquartile range. In contrast, SSM produced a median RMSE of 0.104 m^3/m^3, similar to its overall RMSE and significantly higher ($p < 0.05$) than those of the other products. All products showed negative shifts in median bias relative to their overall bias. GSSM yielded a small negative median bias (−0.014 m^3/m^3), despite overestimating soil moisture on average. As expected, the median ubRMSE values were markedly smaller than the overall ubRMSE values after removing grid-cell-specific biases. The grid-cell-level ubRMSEs for GSSM, GLASS, DSMAP, and SSM were 0.056 m^3/m^3, 0.054 m^3/m^3, 0.063 m^3/m^3, and 0.068 m^3/m^3, respectively, approaching the 0.06 m^3/m^3 target commonly set for high-resolution radar-based soil moisture retrievals.

Fig. 3 also presents the results for the extra grid cells. The core grids achieved higher R values than the extra grids for the three machine-learning-based products (SSM, GSSM, and GLASS), with statistically significant differences between SSM and GLASS. Although only GLASS was trained using filtered stations (Zhang et al., 2023), the training networks used for SSM and GSSM also consisted of well-established monitoring stations with substantially better spatial representativeness. This partly explains why these products had higher correlations at the core grid cells.

The differences between core and extra grids are more complex for RMSE and ubRMSE. DSMAP and GLASS showed slightly lower median RMSEs at the core grids, whereas SSM and GSSM performed marginally better at the extra grids; however, none of these differences were statistically significant. The boxplots for all grid cells are also provided in Fig. 3. The median values show no significant differences compared with those derived separately from the core and extra grids. Accordingly, subsequent evaluations across landcover types, climate zones, and soil-texture classes were conducted using all grid cells to ensure sufficient sample sizes and more reliable statistics. Only correlation coefficients were used for this stratified analysis, as they are considered less sensitive to spatial representativeness effects (Meng et al., 2024a; Wang et al., 2024).

3.2. Performance under different environmental conditions

The performance of the four products varied substantially across the evaluated landcover types (Fig. 4a), reflecting the differing sensitivities of their underlying algorithms to surface heterogeneity. In cropland regions, DSMAP and GSSM showed stronger agreement with the in-situ measurements, with DSMAP achieving a median correlation of approximately 0.600. SSM maintained a more moderate but stable median correlation of about 0.351. GLASS exhibited a relatively high central tendency but a wider performance spread, suggesting that it may be more susceptible to local variations in crop phenology or irrigation practices. In forested areas, the influence of vegetation density and canopy structure became more pronounced. DSMAP's performance declined to a median correlation of 0.372, which can be attributed to the high attenuation of L-band passive microwave signals in dense forests and the reduced sensitivity of thermal-inertia-based methods under substantial vegetation cover. In contrast, GLASS achieved comparable correlations in cropland (0.452) and forest (0.432), indicating that its algorithm may better account for the effects of dense canopy cover.

Grassland represented a high-performance zone for nearly all products. GSSM reached its peak median correlation of 0.574, closely followed by GLASS (median $R = 0.541$). In contrast to the SPL2SMP_E, DSMAP achieved a significantly lower ($p < 0.05$) median correlation on grassland (0.502) than on cropland (0.600). This pattern reflects the nature of the thermal-inertia downscaling approach, which infers soil moisture from diurnal LST amplitude stratified by NDVI. Its accuracy therefore depends on the strength of the coupling between LST dynamics and near surface soil moisture. Croplands often experience irrigation, tillage, and bare soil periods that produce large diurnal temperature swings strongly correlated with soil moisture, enabling more stable

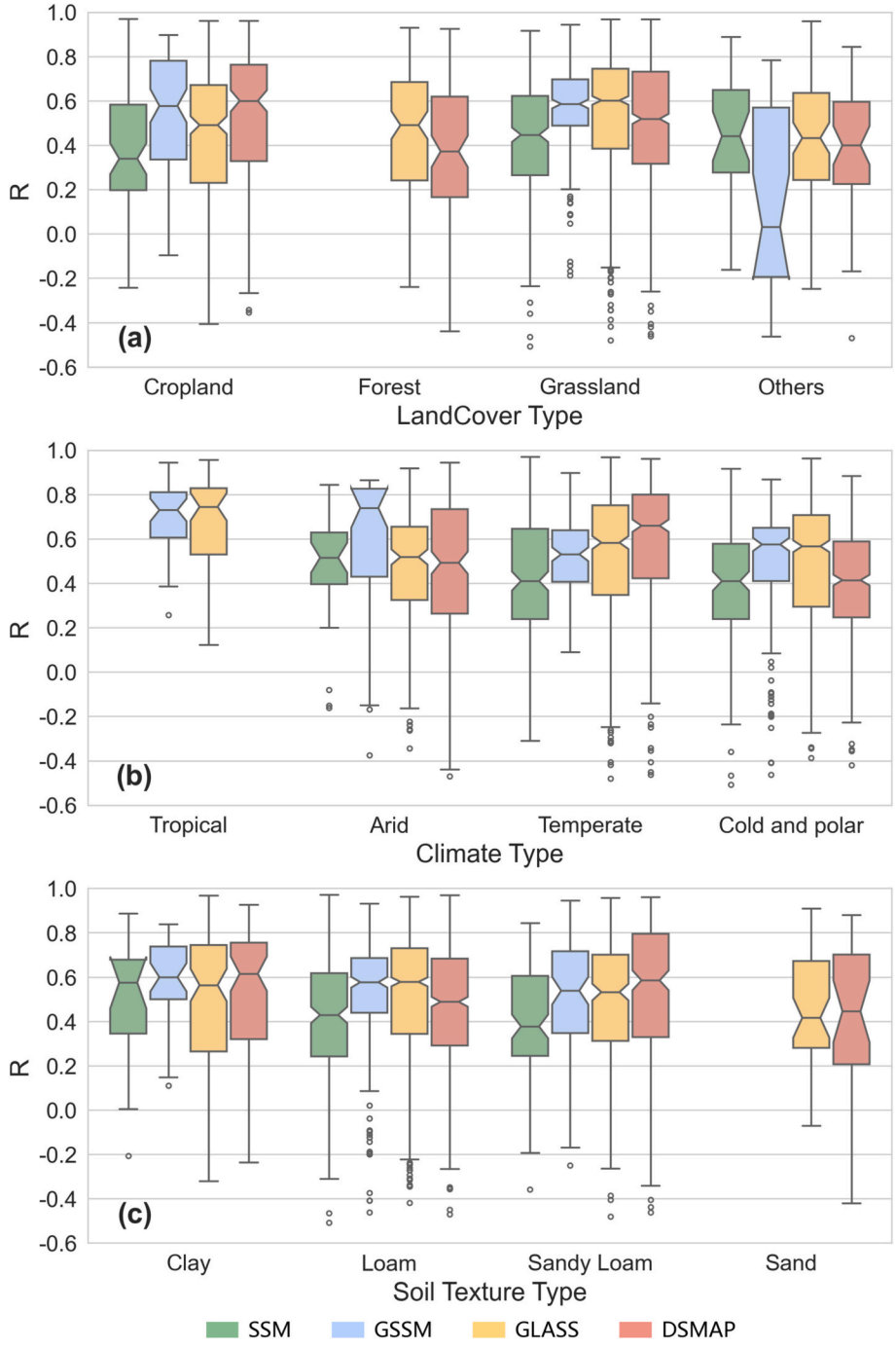

Fig. 4. Performance of four products on (a) four landcover types, (b) four climate zones and (c) four soil texture types.

empirical regressions. Grasslands, by contrast, typically maintain continuous vegetation cover, which dampens diurnal LST amplitude and reduces the sensitivity of the downscaling relationship, leading to lower accuracy.

The "others" category (wetland, urban areas, and water surface) highlights a critical divergence in product reliability and algorithmic robustness due to the substantial surface complexity. While SSM, GLASS, and DSMAP maintain relatively consistent performance, GSSM experiences a pronounced degradation. Its median correlation drops to approximately 0.1, accompanied by a markedly larger interquartile range that extends into negative correlation values. Although GSSM performs strongly in cropland and grassland, these results indicate that it lacks the generalizability required for accurate soil moisture retrieval in more complex or heterogeneous landscapes.

Fig. 4b shows the grid-specific correlations across different climate zones. In tropical regions, all products exhibited high median correlations. GLASS achieved a slightly higher median R (0.745) compared with GSSM (0.730) and DSMAP (0.728). More importantly, all three products performed best in the tropics, a region that is typically challenging for dedicated soil moisture missions such as SMAP and SMOS. Tropical environments are characterized by strong diurnal LST cycles and tight coupling between rainfall and near-surface soil moisture. These conditions help explain why DSMAP can still perform well, even though SMAP's microwave signal is heavily attenuated by humid, high-biomass canopies. Similarly, the machine learning models used in GLASS and GSSM can leverage surface-temperature dynamics, rainfall

history, and vegetation indices to infer soil moisture, allowing them to maintain strong performance despite the reduced sensitivity of remote sensing observations in these regions.

In arid regions, GSSM performed best, achieving a median correlation of 0.740, which was significantly higher than that of the other products. However, GSSM still substantially overestimated the soil moisture in these regions as shown in Fig. 2e. SSM, GLASS, and DSMAP showed more moderate median correlations ranging from 0.49 to 0.52, with DSMAP exhibiting the widest variability and a larger number of negative grid-cell correlations. This is likely attributable to the large temperature fluctuations that are weakly related to soil moisture. In temperate regions, DSMAP achieved the highest median correlation (0.660), statistically outperforming both SSM and GSSM. GLASS followed closely, although its wider interquartile range indicates less consistency across grid cells.

In cold and polar regions, the performance of all products converged, with median correlations ranging from 0.38 to 0.58. Although GSSM maintained a slight advantage in this zone, the differences were not statistically significant. DSMAP showed the lowest median correlation (0.38), which can be attributed to the fact that frozen soils, snow cover, and weak diurnal temperature cycles suppress both microwave sensitivity and thermal-inertia signals, thereby breaking the physical link between surface observations and soil moisture. Overall, GSSM and GLASS remained the most robust across diverse climate regimes, with GSSM's advantage being most pronounced in arid environments.

Fig. 4c presents the grid-specific correlations of the four products across different soil-texture classes. In clay soils, DSMAP achieved the highest median correlation (0.615), followed closely by GSSM (0.599), SSM (0.575), and GLASS (0.564). In loam soils, GLASS exhibited the highest median correlation (0.578), with GSSM following closely at 0.576; both products were statistically superior to SSM, whose median correlation dropped to 0.42. Sandy-loam soils showed a similar pattern, with DSMAP reaching its peak performance in this texture class (median $R = 0.585$). The substantial spread and numerous outliers—particularly for GSSM in loam—indicate that although median performance is high, local soil heterogeneity and differences in moisture-retention properties can lead to occasional retrieval inaccuracies.

In sandy soils, only GLASS and DSMAP were represented. GLASS achieved a median correlation of 0.416, whereas DSMAP showed a slightly higher median (0.445) but a much broader distribution, including several negative outliers. Both products exhibited their poorest performance in sandy soils among the four texture classes, consistent with the pronounced overestimation at low soil moisture values observed in Fig. 2.

4. Intercomparison with airborne soil moisture

4.1. North America

During SMAPVEX12 (Fig. 5), airborne data revealed a distinct spatial distribution of soil moisture, with wetter conditions in the southeast and drier conditions in the northwest. On June 15, airborne soil moisture ranged from 0.07 to 0.55 m^3/m^3, with a mean of 0.22 m^3/m^3. SSM demonstrated relatively poor agreement with the airborne observations, with a low correlation of 0.152 and an RMSD of 0.116 m^3/m^3, indicating limited spatial variability and a relatively uniform spatial pattern. In contrast, GSSM and GLASS better captured the regional variations. The dynamic ranges of GSSM and GLASS were 0.14–0.38 m^3/m^3 and 0.13–0.45 m^3/m^3 respectively. Following heavy rainfall on June 16, soil moisture increased sharply before gradually declining until July 3, with the airborne data on June 17 showing a substantial rise in the southeast and an increase in the mean near-surface soil moisture from 0.29 to 0.42 m^3/m^3. SSM had a small increase in the average soil moisture value (0.06 m^3/m^3), but with a large bias of −0.15 m^3/m^3. GLASS provided a closer mean (0.37 m^3/m^3) but slightly underestimated the magnitude of change (0.01 m^3/m^3). During the subsequent drying period (June 17–July 3), the average airborne soil moisture decreased from 0.28 to 0.12 m^3/m^3. All products captured this trend, but with differing dynamic ranges. GLASS (0.31 to 0.19 m^3/m^3) exhibited a variation that was most consistent with the airborne observations, whereas SSM (0.25 to 0.19 m^3/m^3) showed a more limited variation. This contrast is consistent with the accuracy metrics reported in Table 3 for SMAPVEX12, where a higher correlation was achieved for GLASS (0.387) than SSM (0.152). A minor rainfall event on July 12 led to an increased soil

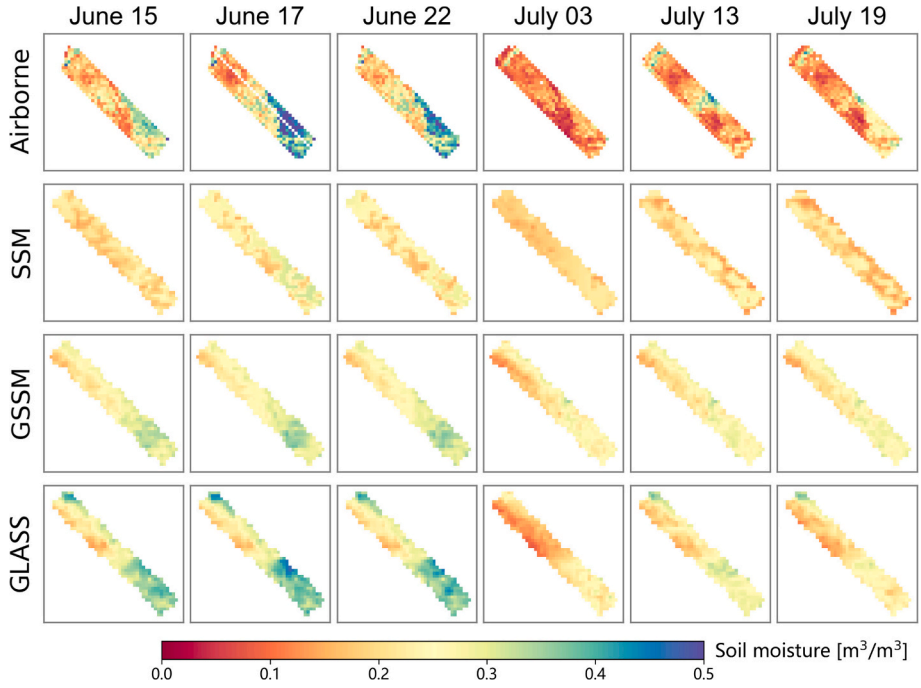

Fig. 5. Spatial patterns of soil moisture derived from SSM, GSSM and GLASS products in comparison with aircraft observations throughout the SMAPVEX12 field campaign.

Table 3
Evaluation results of SSM, GSSM, GLASS and DSMAP product against airborne observations of soil moisture during the field campaign.

Product	Metrics	SMAPVEX12	SMAPVEX15	SMAPVEX16-IA	SMAPVEX16-MB	SMAPEx-4	SMAPEx-5
SSM	R	0.152	0.316	−0.065	0.152	0.131	0.441
	Bias (m^3/m^3)	0.007	−0.051	−0.016	0.074	−0.001	0.032
	RMSD (m^3/m^3)	0.116	0.081	0.09	0.122	0.112	0.157
GSSM	R	0.358	0.409	0.32	0.251	0.1	0.426
	Bias (m^3/m^3)	−0.067	0.014	0.014	0.023	0.008	0.041
	RMSD (m^3/m^3)	0.121	0.058	0.07	0.093	0.114	0.163
GLASS	R	0.387	0.426	0.384	0.219	0.119	0.406
	Bias (m^3/m^3)	−0.88	0.003	−0.029	0.017	0.008	−0.035
	RMSD (m^3/m^3)	0.138	0.056	0.075	0.105	0.112	0.157
DSMAP	R		0.527	0.518	0.411	0.747	0.665
	Bias (m^3/m^3)		−0.012	0.025	−0.010	−0.034	0.004
	RMSD (m^3/m^3)		0.132	0.075	0.092	0.067	0.131

moisture in the central and southern regions on July 13, which was effectively captured only by GLASS. In view of the statistics in Table 3, all three products showed a low correlation with the airborne soil moisture during SMAPVEX12, with the highest R reaching only 0.387 (GLASS). While GLASS had the strongest temporal consistency, it also showed the largest overall spatial bias (−0.088 m^3/m^3) and RMSD (0.138 m^3/m^3).

Fig. 6 compares the airborne soil moisture observations with the four satellite-derived soil moisture products during SMAPVEX15, a campaign conducted under predominantly dry conditions. Following a rainfall event on August 8, airborne soil moisture showed a sharp increase in the central region, with the average soil moisture increasing from 0.079 m^3/m^3 on August 5 to 0.151 m^3/m^3 on August 8. GLASS captured this wetting trend most closely, with an increase of 0.041 m^3/m^3, followed by GSSM (0.033 m^3/m^3), while SSM showed a minimal response (0.016 m^3/m^3), indicating low sensitivity to precipitation. After August 8, the study area exhibited an overall drying trend, with mean soil moisture decreasing from 0.151 m^3/m^3 to 0.063 m^3/m^3. DSMAP reproduced this trend most accurately, with a variation from 0.155 m^3/m^3 to 0.083 m^3/m^3, closely matching the airborne range. GLASS showed a moderate decline (0.19–0.31 m^3/m^3), while GSSM exhibited the smallest change (0.121–0.085 m^3/m^3). However, SSM failed to reflect the drying trend, maintaining a narrow range (0.173–0.142 m^3/m^3) and consistently overestimated soil moisture.

During the SMAPVEX15, DSMAP best captured both the spatial variability and temporal dynamics, showing the highest correlation with airborne data (0.527). However, it also had the largest RMSD (0.132 m^3/m^3), indicating greater variability and potential overestimation. GLASS and GSSM performed comparably well, with moderate correlations (0.426 and 0.409, respectively) and the lowest RMSD values (0.056 and 0.058 m^3/m^3), suggesting better overall accuracy. Both products effectively identified dry regions but underestimated the central wet zones and showed compressed dynamic ranges. SSM performed the poorest, with the lowest correlation (0.316) and limited spatial responsiveness, consistently overestimating soil moisture and failing to capture both dry and wet extremes.

Fig. 7 compares the four products with airborne observations during the SMAPVEX16 campaign at the Iowa and Manitoba sites. At the Iowa site (Fig. 7a), airborne data showed a large soil moisture decrease from 0.294 to 0.133 m^3/m^3 between June 1–3. All three long-record products detected this drying, but they all substantially overestimated the soil moisture content. However, the same dry patches in SSM were not

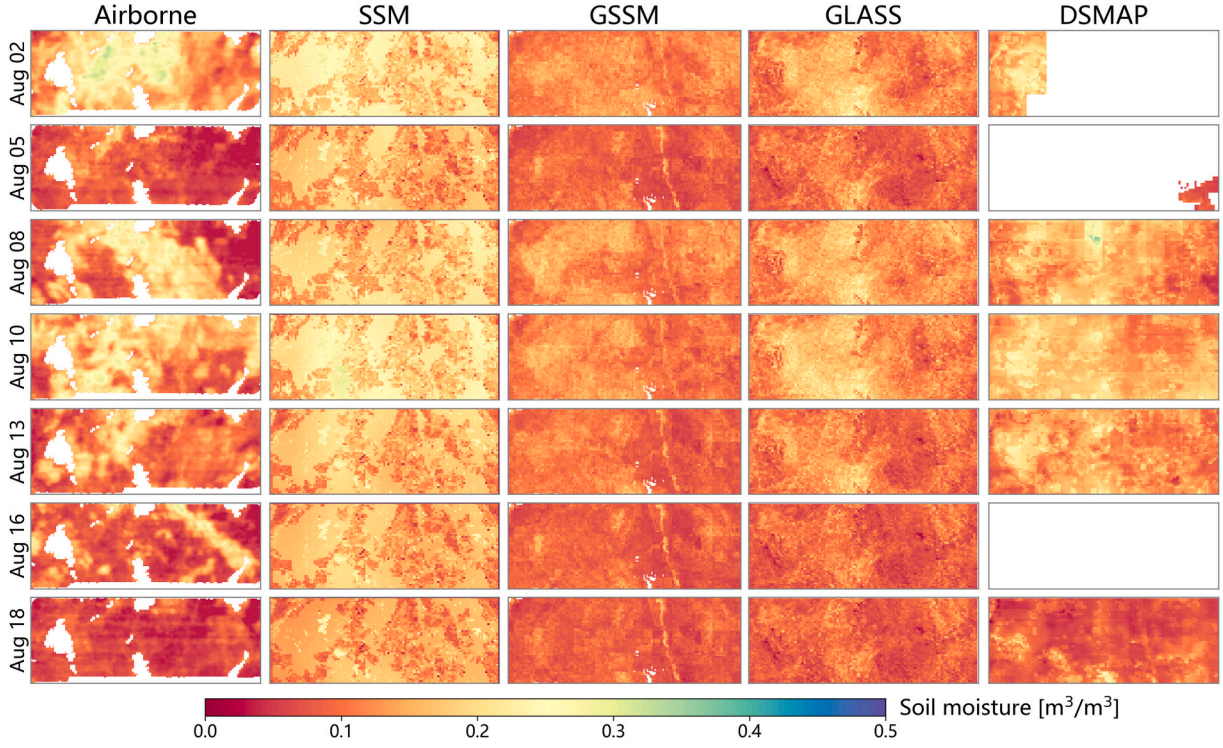

Fig. 6. Same as Fig. 5 but for SMAPVEX15.

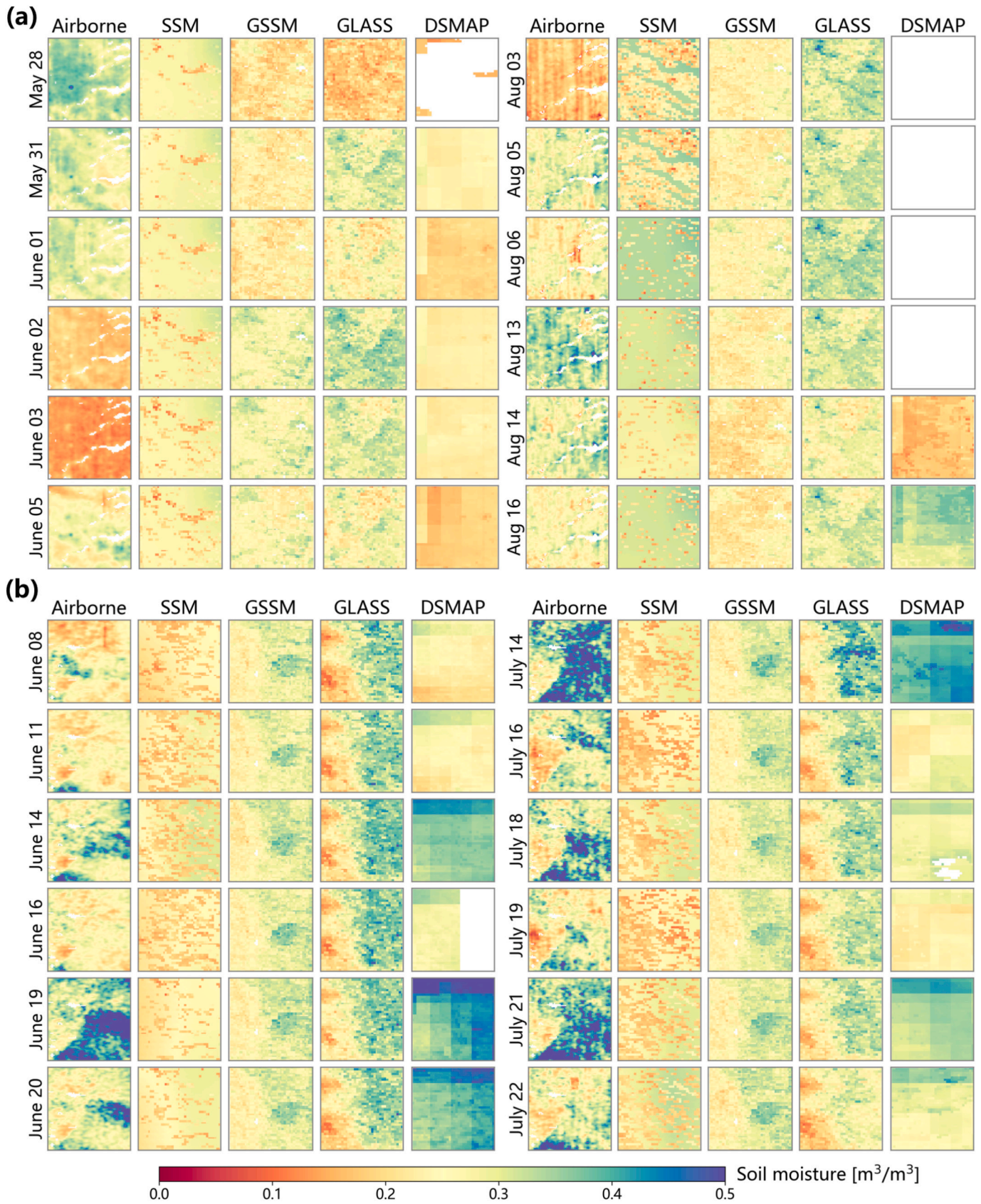

Fig. 7. Comparison of soil moisture patterns from SSM, GSSM, GLASS, DSMAP, and airborne observations during the SMAPVEX16 field campaign: (a) Iowa, where urban and riparian areas appear white in the airborne data; and (b) Manitoba, where urban areas appear white.

observed during the drying period. During the second Iowa period (August 3–14), airborne soil moisture followed a dry–wet–dry cycle, peaking at 0.33 m^3/m^3. GLASS most accurately tracked this evolution, with both the dynamic range (0.183–0.32 m^3/m^3) and spatial patterns closely aligning to the aircraft data. GSSM captured the initial wetting but underestimated the subsequent drying (0.003 m^3/m^3 change vs. 0.04 m^3/m^3 airborne). DSMAP showed muted responses to rainfall (0.163–0.238 m^3/m^3), while SSM again performed the worst, remaining nearly static (0.257–0.27 m^3/m^3) and spatially uniform.

At the Manitoba site (Fig. 7b), multiple rainfall events (June 14, 19; July 18, 21) caused a pronounced soil moisture increase (Qian et al., 2025), especially in the clay-rich southeast where water retention is high. DSMAP most faithfully reproduced these episodic wettings and maintained a good agreement with the airborne measurements. However, clear patches of 9 km grids can be observed in the DSMAP images. This occurs because the downscaling approach redistributes coarse-resolution soil moisture using high-resolution auxiliary patterns and thus retains strong dependence on the original coarse grid, particularly in areas with low surface heterogeneity. As a result, although DSMAP performed well in capturing temporal dynamics, its spatial fidelity was limited. GLASS captured the broad east–west moisture variations and matched the airborne dynamic range (0.08–0.52 vs. 0.03–0.56 m^3/m^3) but responded weakly to individual storms. Moreover, GLASS and GSSM consistently maintained drier conditions in the western part of the study area throughout the experiment, exhibiting narrow dynamic ranges of 0.237–0.244 m^3/m^3 and 0.151–0.208 m^3/m^3, respectively. Furthermore, the spatial extent of the dry zones was similar to the distribution of sand and sandy loam in the west, indicating a relatively poor performance of GLASS over sand. SSM lagged overall, showing limited spatial variability and failing to reflect rainfall impacts.

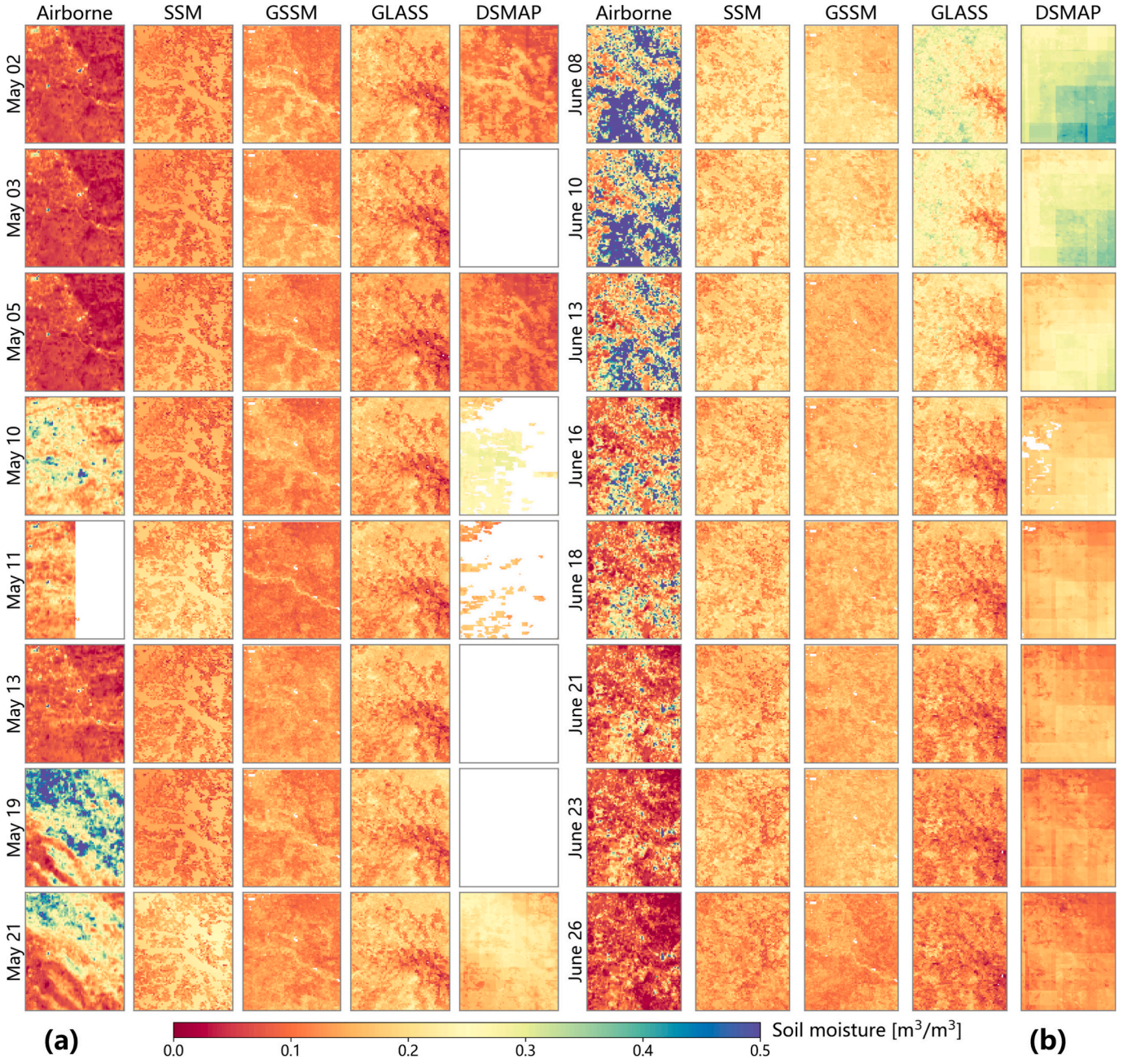

Fig. 8. Comparison of soil moisture distributions patterns from SSM, GSSM, GLASS, DSMAP, and airborne observations during (a) SMAPEx-4; and (b) SMAPEx-5.

4.2. Australia

Fig. 8 compares airborne soil moisture observations with the four products during the SMAPEx-4 (a) and SMAPEx-5 (b) campaigns. SMAPEx-4 began under spatially homogeneous dry conditions, followed by small to moderate rainfall events on May 9 and 18 that increased surface heterogeneity. Among the products, DSMAP showed the best overall performance, with an RMSD of 0.067 m^3/m^3, effectively capturing both the spatial distribution and the temporal dynamics. On May 10, DSMAP closely followed the airborne wetting trend, with a mean soil moisture of 0.252 m^3/m^3, compared to airborne values ranging from 0.06 to 0.201 m^3/m^3. In contrast, SSM, GSSM and GLASS failed to represent the rainfall-induced changes, showing limited dynamic ranges. This limitation likely resulted from cloud contamination affecting the optical remote sensing inputs used in these products, as imperfect cloud masking (Zhu and Woodcock, 2012) can lead to residual atmospheric artifacts and data gaps that propagate uncertainty into the derived soil moisture estimates (Zhong et al., 2024).

Among them, GSSM performed the worst, with a narrow range (0.11–0.137 m^3/m^3) and an RMSD of 0.114 m^3/m^3. SSM and GLASS showed moderate improvements, but still underestimated the post-rainfall soil moisture, with dynamic ranges of 0.176–0.183 m^3/m^3 and 0.128–0.161 m^3/m^3, respectively.

Compared to SMAPEx-4, SMAPEx-5 began with wet and heterogeneous soil due to extensive rainfall prior to the experiment (Ye et al., 2019). As no further rainfall occurred, the full transition of SM from wet to dry (0.367 to 0.074 m^3/m^3) was clearly observed.

All four products captured the overall drying trend, but SSM and GSSM showed limited responsiveness, with small changes in magnitudes (0.06 m^3/m^3) and a high RMSD (0.157 and 0.163 m^3/m^3, respectively). In contrast, GLASS and DSMAP displayed wider dynamic ranges. DSMAP most closely matched the airborne data, with a dynamic range of 0.317–0.127 m^3/m^3 and an RMSD of 0.131 m^3/m^3. Spatially, GLASS better captured wet conditions in the western and northern regions, while DSMAP more accurately represented wetter areas in the eastern and southern parts. However, GLASS exhibited a distinct dry zone in the southeastern part of the study area, characterized by a narrow soil moisture range (0.091–0.131 m^3/m^3) and low spatial variability. This pattern may be attributed to the hilly terrain of the region; affected by topographic variability, the GLASS algorithm performed relatively poorly under complex topographic conditions.

5. Discussion

Overall, the results reveal clear differences in performance among the four soil moisture products across evaluation scales. GLASS and GSSM generally show stronger agreement with in-situ observations, while DSMAP demonstrates advantages in capturing spatial and temporal dynamics when compared with airborne data. In contrast, SSM consistently exhibits limited sensitivity to both extremes and variability. Performance also varies substantially across environmental conditions, with notable dependencies on land cover, climate regime, and soil texture Building on these findings, the discussion is organized around three objectives and knowledge gaps: evaluating real-world performance beyond official reports, assessing spatial patterns using airborne references, and providing practical guidance for users and developers.

5.1. Limitations and generalization challenges revealed by independent evaluation

The four evaluated products performed more poorly within the core grid cells (Fig. 2) than what was reported in their respective documentation. For example, SSM was officially reported to have an ubRMSE of 0.045 m^3/m^3 (Zheng et al., 2023), yet in this study its ubRMSE was found to be 0.104 m^3/m^3, with a bias reaching −0.038 m^3/m^3, deviating substantially from the reported zero bias. This discrepancy may result from the reliance on ESA-CCI soil moisture and ERA5 reanalysis for downscaling, which could introduce bias under regions with sparse in-situ observations. GSSM achieved an RMSE of 0.10 m^3/m^3, being nearly twice its reported value of 0.05 m^3/m^3 (Han et al., 2023), indicating limited cross-regional generalization capability despite being driven by predictors with clear physical relevance to soil moisture dynamics. GLASS showed a relatively consistent performance, with an RMSE of 0.105 m^3/m^3, which is close to its reported value of 0.079 m^3/m^3 (Zhang et al., 2023), likely reflecting the stabilizing effect of ETC-based station selection and the robustness of the XGBoost model. In contrast, DSMAP was reported to have an ubRMSE of 0.063 m^3/m^3 (Fang et al., 2022), but was found to have an ubRMSE of 0.099 m^3/m^3. This is consistent with the known limitations of thermal inertia-based downscaling in regions where soil moisture and surface temperature are weakly coupled. Overall, the performance degradation observed across products largely reflects two factors: overfitting to the official validation environments and the reduced physical sensitivity of key input features when applied to independent regions with different climate, vegetation, and soil conditions.

The comparison between core and extra grid cells (Fig. 3) further reveals the influence of spatial representativeness on product evaluation. Core grid cells, where the in-situ station's land cover is more representative of the surrounding 1 km grid, reduce the mismatch between point-scale measurements and grid-scale estimates, leading to a more reliable assessment of product performance. In contrast, extra grid cells are more affected by sub-grid heterogeneity. The higher correlations observed in core grid cells for machine-learning-based products (SSM, GSSM, and GLASS) suggest that these products are more capable of capturing soil moisture dynamics in areas with low surface heterogeneity. For DSMAP, the absence of significant difference in correlation between core and extra grid cells likely reflects the fact that its thermal-inertia-based downscaling approach is less dependent on local land-cover homogeneity. These findings highlight the need to include diverse, heterogeneous site conditions in both model training and independent evaluation, so that reported accuracies are representative of real-world applications rather than limited to homogeneous landscapes.

Substantial discrepancies were also observed between evaluations using different grid cell definitions. Performance over the core grid cells defined in this study was compared with results from a stricter definition requiring more than five in-situ stations per grid cell. All products showed improved performance under this stricter definition (Supplementary Material), with SSM exhibiting the largest improvement, achieving an R of 0.585 and an RMSE of 0.082 m^3/m^3 (Fig. S6a). A similar pattern was reported for the GLASS product, where performance on extended triple collocation (ETC)-selected sites was substantially better than on excluded sites (Zhang et al., 2023). These differences arise because strict site selection greatly reduces sub-grid representativeness error. Grid cells with dense in-situ sampling provide a more accurate approximation of the true 1 km soil moisture mean, thereby inflating apparent accuracy. However, such strict sites represent only a very small fraction of the land surface (e.g., only five grid cells for SSM in Supplementary Material), and their environmental conditions are typically homogeneous and well-instrumented. As a result, while accuracy on these sites is more reliable, it is less informative for independent evaluation and offers limited insight into model performance in heterogeneous or complex regions.

Even with the broader core grid definition adopted in this study, the evaluated grid cells still cover only a small portion of the global land surface and remain subject to uncertainties in spatial representativeness. Consequently, the evaluation results may be substantially influenced when generalized across diverse climates and landcover conditions (Min et al., 2023; Peng et al., 2025), and should therefore be interpreted as reflecting product performance within the studied regions rather than being generalized to the global scale. While this study reveals performance limitations under specific conditions, further validation across more diverse and spatially extensive observational networks is required

to more comprehensively characterize the products' global error characteristics. Nevertheless, these findings indicate that none of the evaluated products met the target accuracies of 0.04 m^3/m^3 for radiometer-based (Brown et al., 2013) and 0.06 m^3/m^3 for radar-based soil moisture retrievals (Colliander et al., 2017b) under the tested machine learning frameworks. This suggests a limited generalization capability of machine learning methods and empirical regressions when applied to environmental conditions not fully represented in the original training data, highlighting the need for independent evaluation and a cautious use of these products in real-world applications.

5.2. Implications from the intercomparison with airborne data

The airborne soil moisture estimates provided a spatially continuous reference that revealed notable differences in how well each product captured fine-scale spatial patterns, offering insights that cannot be obtained from point-based in-situ validation alone, thereby providing a more process-relevant basis for their application in hydrological and ecological studies. Among the evaluated products, DSMAP demonstrated the best overall performance in capturing both spatial distribution patterns and temporal dynamics of soil moisture (Figs. 6–8 and Table 3). It successfully captured the soil moisture increase after precipitation events and maintained a dynamic range closely aligned with airborne observations. This is largely attributed to the high quality of the original SPL2SMP_E dataset, which provides reliable soil moisture dynamics in both space and time. However, as the 1 km DSMAP product is derived through downscaling from the SPL2SMP_E data used on a 9 km grid, residual coarse-resolution spatial patterns remain evident, manifested as distinct grid artifacts in the outputs, which limit its ability to capture fine-scale spatial heterogeneity. This may introduce spatial discontinuities in catchment-scale hydrological models, potentially misrepresenting lateral flow or localized saturation zones (Minet et al., 2011).

GLASS generally performed well across the airborne campaigns, but showed notable underestimation in areas with complex topography (e.g., hilly terrain in Fig. 8b) and sandy soils (Fig. 7b), along with relatively low spatial variability. In contrast, GSSM and SSM exhibited more pronounced limitations. While GSSM captured broad drying and wetting trends in some cases (e.g., SMAPVEX12), its dynamic range was consistently narrow, failing to reflect rainfall-driven spatial variations in soil moisture. SSM performed the poorest overall (Table 3), characterized by low spatial contrast correlation (0.188), limited dynamic range, and higher RMSD values than the other products, with an average RMSD of 0.113 m^3/m^3. These deficiencies prevented it from adequately representing the true spatial heterogeneity of soil moisture observed in airborne measurements. The narrow dynamic range and low spatial contrast observed in SSM and GSSM limit their utility for ecological monitoring. For example, they may fail to trigger the soil moisture thresholds required to identify localized plant water stress or map drought-resilient refugia (Fu et al., 2024).

A common issue across the three machine-learning-based products was the presence of nearly “frozen” spatial patterns, where certain areas remained persistently wetter or drier regardless of rainfall events. While the internal mechanisms of these models cannot be fully diagnosed due to their black-box nature, such behavior is likely driven by their heavy reliance on static predictors (e.g., terrain attributes, soil texture) and on input variables with limited sensitivity to short-term rainfall. As a result, the models tend to preserve stable spatial contrasts even during wetting events, leading to muted temporal variability and an underrepresentation of event-scale soil moisture dynamics.

Although this study made an effort to evaluate spatial patterns, the methods applied were primarily based on visual interpretation and overall accuracy statistics. These approaches provide only qualitative insights and do not offer quantitative measures of how well each product captures spatial variability. Accordingly, key aspects such as pattern similarity, spatial structure, and fine-scale heterogeneity remain unassessed. Future research should incorporate more rigorous spatial evaluation techniques to better characterize the spatial performance of high-resolution soil moisture products. Enhancing spatial-scale evaluation will improve the reliability and practical applicability of these datasets in hydrological modeling, drought monitoring, and agricultural management.

5.3. Guidance for end users and future development of soil moisture products

The four evaluated products had distinct strengths, and no single dataset is universally optimal. GLASS generally provided the most balanced performance, achieving the highest correlation (0.575) and lowest ubRMSE (0.097 m^3/m^3) among the products in the core grid cells (Fig. 2), DSMAP also performed strongly, particularly in capturing temporal dynamics, though its spatial fields sometimes retained coarse-resolution artifacts (Fig. 7 and 8). GSSM showed comparable overall accuracy with smallest overall bias (−0.019 m^3/m^3) and median bias (−0.014 m^3/m^3) but suffered from a narrow dynamic range and the largest bias (0.164 m^3/m^3) during dry extremes (Fig. 2). SSM consistently performed the poorest, with low overall correlation (0.399) and median correlations (< 0.5) (Fig. 2 and 3), limited spatial variability, and weak sensitivity to wetting and drying events. Look up figures were provided (Fig. 9) for end users to identify the best-performing product for a specific landcover type, soil texture, and climate zone. However, only six environmental categories exhibited significantly superior products, highlighting the need to further enhance the accuracy of these products. Fig. 9 may also serve as a reference for deriving fusion weights in the development of a composite product, which is expected to result in an enhanced product.

Apart from a fusion framework of existing products, clear priorities were identified for the observed systematic limitations. A recurring issue across the four products is the imbalance of bias across different soil-moisture ranges, with substantial overestimation at dry conditions and underestimation at wet conditions (Fig. 2e). This reflects several interacting factors. Extremes occur in environments where remote sensing sensitivity is inherently low: very dry conditions are often associated with sandy soils or frozen surfaces, while very wet conditions frequently coincide with dense vegetation that attenuates both microwave and thermal inertia signals. These physical limitations make both ends of the soil moisture spectrum more difficult to retrieve accurately (Fig. 4b and c). In addition, dry and wet extremes were generally underrepresented in the training data due to fewer extreme dry or wet ground measurements, meaning that learning algorithms devote less attention to these cases during optimization. Beyond these environmental and sampling constraints, data-driven models also tend to regress toward the mean, a natural consequence of minimizing global loss functions, which further amplifies the overestimation of dry values and underestimation of wet values. Mitigating the bias imbalance across soil-moisture ranges will require multiple strategies: (1) better representation of extreme environments in the training data; (2) hybrid physical–statistical modeling to improve sensitivity under challenging conditions; and (3) tailored loss functions or post-processing schemes that explicitly preserve the dynamic range rather than regressing toward the mean.

Environmental generalization remains a major challenge. Product performance varied substantially across land-cover types, climate zones, and soil textures, with sharp degradation in heterogeneous landscapes, arid regions, dense forests, and sandy soils (Fig. 4). These patterns highlight the need for training datasets that more fully represent global environmental diversity, as well as model architectures that explicitly incorporate physical constraints to improve transferability beyond well-instrumented regions. Expanding in-situ networks, integrating airborne campaigns, adopting hybrid physical–machine-learning and applying transfer learning approaches (Zhu et al., 2025a; Zhu et al., 2024) will be essential for improving robustness across diverse conditions.

Improving spatial fidelity is another key priority. DSMAP

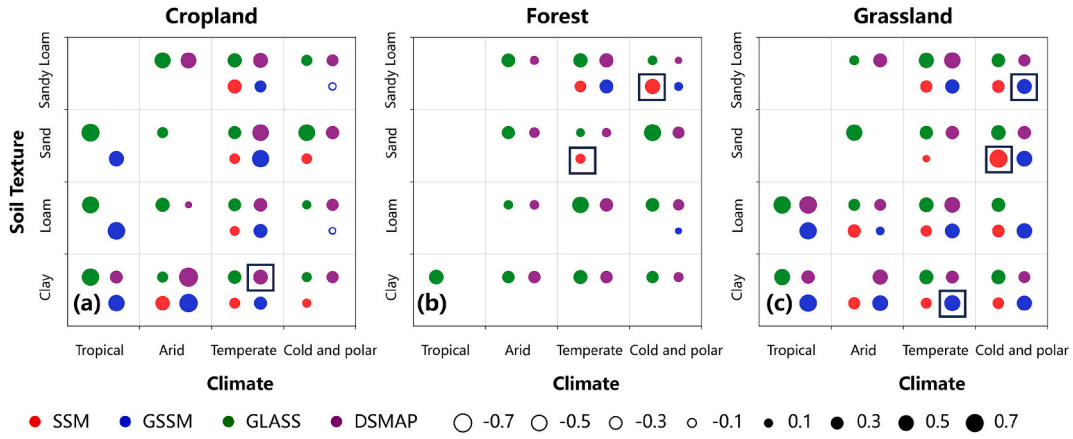

Fig. 9. Correlation coefficients (R) achieved by the four products under a) cropland, b) forest and c) grassland respectively. Only categories with more than five grid cells were included. Circle colors represent the four products, and the circle size reflects the magnitude of R. Circles outlined with black rectangles indicate cases where the product with the highest R value is statistically superior to the others based on a one-sample *t*-test ($p < 0.05$).

demonstrated strong temporal responsiveness but retained coarse-resolution artifacts inherited from the SMAP radiometer product, particularly in regions with low surface heterogeneity. GLASS and GSSM showed muted dynamic ranges and systematic underestimation in sandy soils and complex topography. A related limitation across the data-driven products is the presence of persistent, nearly "frozen" spatial patterns that change little with rainfall. These observations point to a clear trade-off that future development must address. Reliable coarse-resolution inputs such as SMAP products supply valuable temporal information, yet excessive dependence on them can imprint coarse-grid structures onto downscaled fields. Conversely, greater emphasis on high-resolution auxiliary variables improves spatial detail but can amplify systematic errors in challenging environments (e.g., sandy soils, complex terrain). Likewise, heavy use of static predictors (e.g., terrain attributes, soil texture and landcover data) risks locking the retrieval into spatial patterns that are insensitive to short-term hydrologic forcing. Following Meng et al. (2024b), future models should better integrate dynamic, rainfall-responsive information and assign greater weight to predictors that reflect the soil water balance (e.g., low-frequency microwave observations, improved precipitation forcing, and physically informed constraints), while carefully balancing the stabilizing influence of coarse products against the spatial fidelity offered by high-resolution inputs.

6. Conclusions

This study provides a comprehensive assessment of high-resolution soil moisture products by evaluating their real-world performance beyond official validation reports, incorporating spatial validation using airborne observations, and identifying limitations in their generalization and spatial fidelity. The main conclusions are as follows:

1) All four soil moisture products performed more poorly in this independent evaluation than reported in their respective official documentations. None of the products achieved the target ubRMSE of 0.04 m^3/m^3 for radiometer-based retrievals or 0.06 m^3/m^3 for radar-based retrievals. The observed ubRMSE ranged from 0.097 to 0.104 m^3/m^3, highlighting the need for caution when applying these datasets in an operational context.

2) The evaluated products had narrower dynamic ranges (0.10–0.30 m^3/m^3) compared to in-situ observations (0.05–0.40 m^3/m^3). Imbalance of bias was observed with substantial overestimation at dry conditions (> 0.1 m^3/m^3 for 0–0.05 m^3/m^3) and underestimation at wet conditions (< -0.1 m^3/m^3 for 0.40–0.50 m^3/m^3). This indicates a systemic limitation in representing extreme dry and wet conditions, often resulting from machine learning models regressing toward the global mean.

3) Across diverse environmental conditions, the four soil moisture products exhibit distinct strengths and limitations, reflecting the varying sensitivities of their underlying algorithms to land-cover complexity, climate regimes, and soil texture. GLASS and GSSM emerge as the most consistently robust products overall, with GLASS demonstrating strong adaptability across heterogeneous landscapes and GSSM excelling particularly in arid regions and open vegetation types. DSMAP performs well in croplands and certain soil textures but shows reduced reliability in forests, arid climates, and sandy soils due to the inherent constraints of thermal-inertia downscaling and SMAP radiometer sensitivity. SSM generally lags behind the other products, especially in grasslands and loam soils. Notably, GLASS, GSSM, and DSMAP perform exceptionally well in tropical regions, where strong diurnal temperature cycles and tight rainfall–soil moisture coupling enhance retrieval skill despite the challenges faced by traditional microwave missions.

4) Airborne campaigns provided critical insights into spatial performance that the point-based evaluation cannot reveal. DSMAP demonstrated the strongest ability to reproduce wetting and drying trends and maintain temporal consistency. However, it retained distinct 9 km "grid artifacts" inherited from the original SMAP radiometer data, which limit its fine-scale spatial fidelity. GLASS effectively captured broad spatial patterns but underestimated soil moisture in sandy soils and complex terrain. SSM and GSSM showed pronounced limitations, including weak responsiveness to rainfall and poor representation of fine-scale heterogeneity, resulting in a compressed dynamic range and reduced spatial variability. Persistent, nearly "frozen" spatial patterns of soil moisture were observed across the three data-driven based products.

CRediT authorship contribution statement

Yilin Ma: Writing – original draft. **Liujun Zhu:** Writing – review & editing, Writing – original draft, Supervision, Conceptualization. **Shanshui Yuan:** Writing – review & editing. **Junliang Jin:** Writing – review & editing. **Zhengyang Tang:** Writing – review & editing. **Jeffrey P. Walker:** Writing – review & editing.

Declaration of competing interest

The authors declare that they have no known competing financial interests or personal relationships that could have appeared to influence the work reported in this paper.

Acknowledgments

This work was supported by the National Natural Science Foundation of China (42371369, 52525902 and 52279018), the Basic Research Project of Jiangsu Province (BK20250192) and Qing Lan Project. The authors express sincere thanks to the data providers and the International Soil Moisture Network for the network data.

Appendix A. Appendix

Table A1
Summary of the in-situ soil moisture networks used in this study.

Network name	Country/Region	# Station used	Depth used [cm]	Reference
AACES	Australia	19	0–5	(Peischl et al., 2012)
AMMA-CATCH	Benin, Niger, Mali	7	5	(Galle et al., 2018)
ARM	USA	35	2.5, 5	(Cook, 2016)
BIEBRZA_S-1	Poland	27	5	(Musiał et al., 2016)
BNZ-LTER	Alaska	11	5	
COSMOS	USA	2	0–5, 0–4	(Zreda et al., 2008)
COSMOS-UK	UK	21	5	(Cooper et al., 2021)
CTP_SMTMN	China	57	0–5	(Yang et al., 2013)
DAHRA	Senegal	1	5	(Tagesson et al., 2015)
FLUXNET-AMERIFLUX	USA	5	2, 5	
FMI	Finland	26	2, 5	(Ikonen et al., 2018)
FR_Aqui	France	5	1, 5	(Al-Yaari et al., 2018)
HOAL	Austria	33	5	(Blöschl et al., 2016)
HOBE	Denmark	32	0-5	(Jensen and Illangasekare, 2011)
HYDROL-NET_PERUGIA	Italy	2	5	
HiWATER_EHWSN	China	174	4	(Kang et al., 2014)
KHOREZM	Uzbekistan	7	0-5	–
MAQU	China	27	5	(Su et al., 2011)
MySMNet	Malaysia	7	0-5	(Kang et al., 2019)
NAQU	China	11	5	(Su et al., 2011)
NGARI	China	23	5	(Su et al., 2011)
ORACLE	France	6	5, 3	
OZNET	Australia	20	0–5	(Smith et al., 2012)
PBO_H2O	USA	154	0–5	(Larson et al., 2008)
REMEDHUS	Spain	24	0-5	(González-Zamora et al., 2019)
RISMA	Canada	23	0-5	(Ojo et al., 2015)
RSMN	Romania	20	0-5	
Ru_CFR	Russia	2	5	
SASMAS	Australia	14	0–5	(Rüdiger et al., 2007)
SCAN	USA	1	2.54	(Schaefer et al., 2007)
SD_DEM	Sudan	1	5	(Ardö, 2013)
SKKU	Korea	5	5	(Nguyen et al., 2017)
SMN-SDR	China	34	3	(Zhao et al., 2020)
SMOSMANIA	France	22	5	(Calvet et al., 2016)
SNOTEL	USA	1	0-5	(Leavesley et al., 2010)
SOILSCAPE	USA	127	4, 5	http://soilscape.usc.edu/
SWEX_POLAND	Poland	2	0-2	(Marczewski et al., 2010)
TAHMO	West Africa	4	5	
TERENO	Germany	5	5	(Bogena et al., 2018)
TWENTE	Netherlands	44	5	(van der Velde et al., 2023)
TxSON	USA	40	5	(Caldwell et al., 2019)
UDC_SMOS	Germany	11	5	(Schlenz et al., 2012)
USCRN	USA	115	5	(Palecki and Bell, 2013)
USDA-ARS	USA	4	0–5	(Jackson et al., 2010)
VAS	Spain	2	0-5	http://nimbus.uv.es/
WSMN	UK	4	2.5, 5	(Petropoulos and McCalmont, 2017)
XMS-CAT	Spain	11	5	https://visors.icgc.cat/mesurasols/#9/42.1765/1.1132
iRON	USA	10	5	(Osenga et al., 2021)
Tibet-Obs	China	1	5	(Zhang et al., 2021)
SONTE-China	China	19	0–5	(Wang et al., 2023)
QLB-NET	China	82	5	(Chai et al., 2024)
Genhe	China	24	5	(Jiang et al., 2020)
Saihanba	China	25	5	(Jiang et al., 2020)
Little Washita	USA	31	5	(Yang et al., 2020)
Fort Cobb	USA	17	5	(Yang et al., 2020)
Raam	Netherlands	15	5	(Benninga et al., 2018)
OZNET	Australia	93	0-5	(Smith et al., 2012)

Table A2
The number of available grid cells in each category used in this study.

Environmental condition	Product	Category	N
Landcover	SSM	Forest	6
	SSM	Grassland	299
	SSM	Cropland	78
	SSM	Others	29
	GSSM	Forest	11
	GSSM	Grassland	269
	GSSM	Cropland	26
	GSSM	Others	89
	GLASS	Forest	125
	GLASS	Grassland	912
	GLASS	Cropland	327
	GLASS	Others	88
	DSMAP	Forest	132
	DSMAP	Grassland	1011
	DSMAP	Cropland	229
	DSMAP	Others	75
Climate	SSM	Tropical	0
	SSM	Arid	29
	SSM	Temperate	228
	SSM	Cold and polar	155
	GSSM	Tropical	41
	GSSM	Arid	49
	GSSM	Temperate	142
	GSSM	Cold and polar	163
	GLASS	Tropical	80
	GLASS	Arid	263
	GLASS	Temperate	489
	GLASS	Cold and polar	620
	DSMAP	Tropical	54
	DSMAP	Arid	278
	DSMAP	Temperate	531
	DSMAP	Cold and polar	584
Soil texture	SSM	Clay	32
	SSM	Loam	263
	SSM	Sandy Loam	112
	SSM	Sand	5
	GSSM	Clay	42
	GSSM	Loam	259
	GSSM	Sandy Loam	88
	GSSM	Sand	6
	GLASS	Clay	126
	GLASS	Loam	938
	GLASS	Sandy Loam	281
	GLASS	Sand	107
	DSMAP	Clay	107
	DSMAP	Loam	954
	DSMAP	Sandy Loam	317
	DSMAP	Sand	69

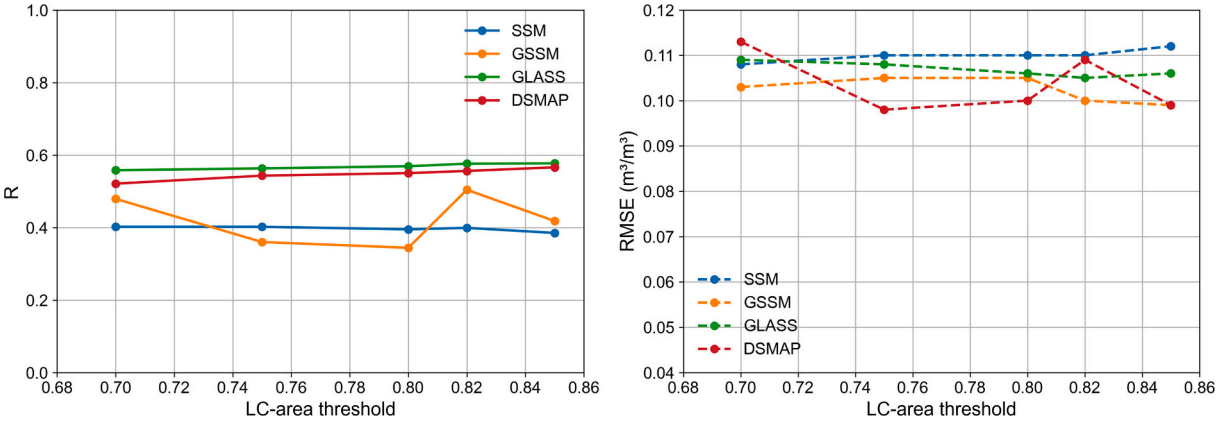

Fig. A1. Sensitivity of accuracy metrics (R and ubRMSE) to different land-cover similarity thresholds (LC-area = 0.70–0.85). The evaluation outcomes are generally insensitive to the choice of threshold, with 0.82 being a literature-based conservative threshold rather than an optimized threshold specific to this study.

Appendix B. Supplementary data

Supplementary data to this article can be found online at https://doi.org/10.1016/j.rse.2026.115534.

Data availability

Data will be made available on request.

References

Al-Yaari, A., Dayau, S., Chipeaux, C., Aluome, C., Kruszewski, A., Loustau, D., Wigneron, J.P., 2018. The AQUI soil moisture network for satellite microwave remote sensing validation in South-Western France. Remote Sens. 10.

Al-Yaari, A., Wigneron, J.P., Dorigo, W., Colliander, A., Pellarin, T., Hahn, S., Mialon, A., Richaume, P., Fernandez-Moran, R., Fan, L., Kerr, Y.H., De Lannoy, G., 2019. Assessment and inter-comparison of recently developed/reprocessed microwave satellite soil moisture products using ISMN ground-based measurements. Remote Sens. Environ. 224, 289–303.

Ardö, J., 2013. A 10-Year Dataset of Basic Meteorology and Soil Properties in Central Sudan. Dataset Papers in Geosciences, 2013, pp. 1–6.

Babaeian, E., Paheding, S., Siddique, N., Devabhaktuni, V.K., Tuller, M., 2021. Estimation of root zone soil moisture from ground and remotely sensed soil information with multisensor data fusion and automated machine learning. Remote Sens. Environ. 260.

Benninga, H.-J.F., Carranza, C.D.U., Pezij, M., van Santen, P., van der Ploeg, M.J., Augustijn, D.C.M., van der Velde, R., 2018. The Raam regional soil moisture monitoring network in the Netherlands. Earth Syst. Sci. Data 10, 61–79.

Blöschl, G., Blaschke, A.P., Broer, M., Bucher, C., Carr, G., Chen, X., Eder, A., Exner-Kittridge, M., Farnleitner, A., Flores-Orozco, A., Haas, P., Hogan, P., Kazemi Amiri, A., Oismüller, M., Parajka, J., Silasari, R., Stadler, P., Strauss, P., Vreugdenhil, M., Wagner, W., Zessner, M., 2016. The hydrological open air laboratory (HOAL) in Petzenkirchen: a hypothesis-driven observatory. Hydrol. Earth Syst. Sci. 20, 227–255.

Bogena, H.R., Montzka, C., Huisman, J.A., Graf, A., Schmidt, M., Stockinger, M., von Hebel, C., Hendricks-Franssen, H.J., van der Kruk, J., Tappe, W., Lücke, A., Baatz, R., Bol, R., Groh, J., Pütz, T., Jakobi, J., Kunkel, R., Sorg, J., Vereecken, H., 2018. The TERENO-Rur hydrological observatory: A multiscale multi-compartment research platform for the advancement of hydrological science. Vadose Zone J. 17.

Brown, M.E., Escobar, V., Moran, S., Entekhabi, D., O'Neill, P.E., Njoku, E.G., Doorn, B., Entin, J.K., 2013. NASA'S soil moisture active passive (SMAP) mission and opportunities for applications users. Bull. Am. Meteorol. Soc. 94, 1125–1128.

Caldwell, T.G., Bongiovanni, T., Cosh, M.H., Jackson, T.J., Colliander, A., Abolt, C.J., Casteel, R., Larson, T., Scanlon, B.R., Young, M.H., 2019. The Texas soil observation network: a comprehensive soil moisture dataset for remote sensing and land surface model validation. Vadose Zone J. 18.

Calvet, J.C., Fritz, N., Berne, C., Piguet, B., Maurel, W., Meurey, C., 2016. Deriving pedotransfer functions for soil quartz fraction in southern France from reverse modeling. Soil 2, 615–629.

Chai, L., Zhu, Z., Liu, S., Xu, Z., Jin, R., Li, X., Kang, J., Che, T., Zhang, Y., Zhang, J., Cui, H., Gao, T., Xu, T., Zhao, S., Pan, X., Guo, G., 2024. A dense soil moisture and freeze-thaw monitoring network in the Qinghai Lake Basin on the Qinghai-Tibetan plateau. Bull. Am. Meteorol. Soc. 105, E584–E604.

Chauhan, N.S., Miller, S., Ardanuy, P., 2003. Spaceborne soil moisture estimation at high resolution: a microwave-optical/IR synergistic approach. Int. J. Remote Sens. 24, 4599–4622.

Chen, Y., Yang, K., Qin, J., Cui, Q., Lu, H., La, Z., Han, M., Tang, W., 2017. Evaluation of SMAP, SMOS, and AMSR2 soil moisture retrievals against observations from two networks on the Tibetan Plateau. J. Geophys. Res.-Atmos. 122, 5780–5792.

Colliander, A., Chan, S., Kim, S.-b., Das, N., Yueh, S., Cosh, M., Bindlish, R., Jackson, T., Njoku, E., 2012. Long term analysis of PALS soil moisture campaign measurements for global soil moisture algorithm development. Remote Sens. Environ. 121, 309–322.

Colliander, A., Njoku, E.G., Jackson, T.J., Chazanoff, S., McNairn, H., Powers, J., Cosh, M.H., 2016. Retrieving soil moisture for non-forested areas using PALS radiometer measurements in SMAPVEX12 field campaign. Remote Sens. Environ. 184, 86–100.

Colliander, A., Cosh, M.H., Misra, S., Jackson, T.J., Crow, W.T., Chan, S., Bindlish, R., Chae, C., Collins, C.H., Yueh, S.H., 2017a. Validation and scaling of soilmoisture in a semi-arid environment: SMAP validation experiment 2015 (SMAPVEX15). Remote Sens. Environ. 196, 101–112.

Colliander, A., Jackson, T.J., Bindlish, R., Chan, S., Das, N., Kim, S.B., Cosh, M.H., Dunbar, R.S., Dang, L., Pashaian, L., Asanuma, J., Aida, K., Berg, A., Rowlandson, T., Bosch, D., Caldwell, T., Caylor, K., Goodrich, D., al Jassar, H., Lopez-Baeza, E., Martínez-Fernández, J., González-Zamora, A., Livingston, S., McNairn, H., Pacheco, A., Moghaddam, M., Montzka, C., Notarnicola, C., Niedrist, G., Pellarin, T., Prueger, J., Pulliainen, J., Rautiainen, K., Ramos, J., Seyfried, M., Starks, P., Su, Z., Zeng, Y., van der Velde, R., Thibeault, M., Dorigo, W., Vreugdenhil, M., Walker, J.P., Wu, X., Monerris, A., O'Neill, P.E., Entekhabi, D., Njoku, E.G., Yueh, S., 2017b. Validation of SMAP surface soil moisture products with core validation sites. Remote Sens. Environ. 191, 215–231.

Colliander, A., Jackson, T.J., Cosh, M., Misra, S., Bindlish, R., Powers, J., McNairn, H., Bullock, P., Berg, A., Magagi, R., O'Neill, P., Yueh, S., & Ieee (2017c). Soil Moisture retrieval with airborne pals instrument over agricultural areas in SMAPVEX16. In, IEEE International Geoscience and Remote Sensing Symposium (IGARSS) (pp. 3949–3952). Fort Worth, TX.

Colliander, A., Cosh, M.H., Misra, S., Jackson, T.J., Crow, W.T., Powers, J., McNairn, H., Bullock, P., Berg, A., Magagi, R., Gao, Y., Bindlish, R., Williamson, R., Ramos, I., Latham, B., O'Neill, P., Yueh, S., 2019. Comparison of high-resolution airborne soil moisture retrievals to SMAP soil moisture during the SMAP validation experiment 2016 (SMAPVEX16). Remote Sens. Environ. 227, 137–150.

Cook, D.R., 2016. Soil temperature and moisture profile (STAMP) system handbook. In: United States: ARM Climate Research Facility, Pacific Northwest National Laboratory, Richland, WA. DOE Office of Science Atmospheric Radiation Measurement (ARM) Program (United States).

Cooper, H.M., Bennett, E., Blake, J., Blyth, E., Boorman, D., Cooper, E., Evans, J., Fry, M., Jenkins, A., Morrison, R., Rylett, D., Stanley, S., Szczykulska, M., Trill, E., Antoniou, V., Askquith-Ellis, A., Ball, L., Brooks, M., Clarke, M.A., Cowan, N., Cumming, A., Farrand, P., Hitt, O., Lord, W., Scarlett, P., Swain, O., Thornton, J., Warwick, A., Winterbourn, B., 2021. COSMOS-UK: national soil moisture and hydrometeorology data for environmental science research. Earth Syst. Sci. Data 13, 1737–1757.

Dandridge, C., Fang, B., Lakshmi, V., 2020. Downscaling of SMAP soil moisture in the lower Mekong River basin. Water 12.

Dorigo, W., Himmelbauer, I., Aberer, D., Schremmer, L., Petrakovic, I., Zappa, L., Preimesberger, W., Xaver, A., Annor, F., Ardo, J., Baldocchi, D., Bitelli, M., Bloeschl, G., Bogena, H., Brocca, L., Calvet, J.-C., Julio Camarero, J., Capello, G., Choi, M., Cosh, M.C., van de Giesen, N., Hajdu, I., Ikonen, J., Jensen, K.H., Kanniah, K.D., de Kat, I., Kirchengast, G., Rai, P.K., Kyrouac, J., Larson, K., Liu, S., Loew, A., Moghaddam, M., Martinez Fernandez, J., Mattar Bader, C., Morbidelli, R., Musial, J.P., Osenga, E., Palecki, M.A., Pellarin, T., Petropoulos, G.P., Pfeil, I., Powers, J., Robock, A., Rudiger, C., Rummel, U., Strobel, M., Su, Z., Sullivan, R., Tagesson, T., Varlagin, A., Vreugdenhil, M., Walker, J., Wen, J., Wenger, F., Wigneron, J.P., Woods, M., Yang, K., Zeng, Y., Zhang, X., Zreda, M., Dietrich, S., Gruber, A., van Oevelen, P., Wagner, W., Scipal, K., Drusch, M., Sabia, R., 2021. The International soil moisture network: serving earth system science for over a decade. Hydrol. Earth Syst. Sci. 25, 5749–5804.

Entekhabi, D., Njoku, E.G., O'Neill, P.E., Kellogg, K.H., Crow, W.T., Edelstein, W.N., Entin, J.K., Goodman, S.D., Jackson, T.J., Johnson, J., Kimball, J., Piepmeier, J.R., Koster, R.D., Martin, N., McDonald, K.C., Moghaddam, M., Moran, S., Reichle, R., Shi, J.C., Spencer, M.W., Thurman, S.W., Tsang, L., Van Zyl, J., 2010. The soil moisture active passive (SMAP) Mission. Proc. IEEE 98, 704–716.

Fan, D., Zhao, T.J., Jiang, X.G., Garcia-Garcia, A., Schmidt, T., Samaniego, L., Attinger, S., Wu, H., Jiang, Y.Z., Shi, J.C., Fan, L., Tang, B.H., Wagner, W., Dorigo, W., Gruber, A., Mattia, F., Balenzano, A., Brocca, L., Jagdhuber, T., Wigneron, J.P., Montzka, C., Peng, J., 2025. A Sentinel-1 SAR-based global 1-km resolution soil moisture data product: algorithm and preliminary assessment. Remote Sens. Environ. 318.

Fang, B., Lakshmi, V., Cosh, M., Liu, P.-W., Bindlish, R., Jackson, T.J., 2022. A global 1-km downscaled SMAP soil moisture product based on thermal inertia theory. Vadose Zone J. 21.

Fu, Z., Ciais, P., Wigneron, J.-P., Gentine, P., Feldman, A.F., Makowski, D., Viovy, N., Kemanian, A.R., Goll, D.S., Stoy, P.C., Prentice, I.C., Yakir, D., Liu, L., Ma, H., Li, X., Huang, Y., Yu, K., Zhu, P., Li, X., Zhu, Z., Lian, J., Smith, W.K., 2024. Global critical soil moisture thresholds of plant water stress. Nat. Commun. 15.

Galle, S., Grippa, M., Peugeot, C., Moussa, I.B., Cappelaere, B., Demarty, J., Mougin, E., Panthou, G., Adjomayi, P., Agbossou, E.K., Ba, A., Boucher, M., Cohard, J.M., Descloitres, M., Descroix, L., Diawara, M., Dossou, M., Favreau, G., Gangneron, F., Gosset, M., Hector, B., Hiernaux, P., Issoufou, B.A., Kergoat, L., Lawin, E., Lebel, T., Legchenko, A., Abdou, M.M., Malam-Issa, O., Mamadou, O., Nazoumou, Y., Pellarin, T., Quantin, G., Sambou, B., Seghieri, J., Séguis, L., Vandervaere, J.P., Vischel, T., Vouillamoz, J.M., Zannou, A., Afouda, S., Alhassane, A., Arjounin, M., Barral, H., Biron, R., Cazenave, F., Chaffard, V., Chazarin, J.P., Guyard, H., Koné, A., Mainassara, I., Mamane, A., Oi, M., Ouani, T., Soumaguel, N., Wubda, M., Ago, E.E., Alle, I.C., Allies, A., Arpin-Pont, F., Awessou, B., Cassé, C., Charvet, G., Dardel, C., Depeyre, A., Diallo, F.B., Do, T., Fatras, C., Frappart, F., Gal, L., Gascon, T., Gibon, F., Guiro, I., Ingatan, A., Kempf, J., Kotchoni, D.O.V., Lawson, F.M.A., Leauthaud, C., Louvet, S., Mason, E., Nguyen, C.C., Perrimond, B., Pierre, C., Richard, A., Robert, E., Román-Cascón, C., Velluet, C., Wilcox, C., 2018. AMMA-CATCH, a critical zone Observatory in West Africa Monitoring a region in transition. Vadose Zone J. 17, 1–24.

González-Zamora, A., Sánchez, N., Pablos, M., Martínez-Fernández, J., 2019. CCI soil moisture assessment with SMOS soil moisture and in situ data under different environmental conditions and spatial scales in Spain. Remote Sens. Environ. 225, 469–482.

Han, Q., Zeng, Y., Zhang, L., Wang, C., Prikaziuk, E., Niu, Z., Su, B., 2023. Global long term daily 1 km surface soil moisture dataset with physics informed machine learning. Sci. Data 10.

IIASA, F, 2023. Harmonized World Soil Database Version 2.0. Rome and Laxenburg.

Ikonen, J., Smolander, T., Rautiainen, K., Cohen, J., Lemmetyinen, J., Salminen, M., Pulliainen, J., 2018. Spatially distributed evaluation of ESA CCI soil moisture products in a northern boreal Forest environment. Geosciences 8.
Jackson, T.J., Cosh, M.H., Bindlish, R., Starks, P.J., Bosch, D.D., Seyfried, M., Goodrich, D.C., Moran, M.S., Du, J.Y., 2010. Validation of advanced microwave scanning radiometer soil moisture products. IEEE Trans. Geosci. Remote Sens. 48, 4256–4272.
Jensen, K.H., Illangasekare, T.H., 2011. HOBE: a hydrological observatory. Vadose Zone J. 10, 1–7.
Jiang, L., Wang, J., Cui, H., Wang, G., Zhao, T., Zhao, S., Chai, L., Liu, X., Yang, J., 2020. In situ soil moisture and temperature network in genhe watershed and saihanba area in China. Data Brief 31, 105693.
Kang, J., Li, X., Jin, R., Ge, Y., Wang, J.F., Wang, J.H., 2014. Hybrid optimal design of the eco-hydrological wireless sensor network in the middle reach of the Heihe River basin, China. SENSORS 14, 19095–19114.
Kang, C.S., Kanniah, K.D., Kerr, Y.H., 2019. Calibration of SMOS soil moisture retrieval algorithm: a case of tropical site in Malaysia. IEEE Trans. Geosci. Remote Sens. 57, 3827–3839.
Kerr, Y.H., Waldteufel, P., Wigneron, J.P., Delwart, S., Cabot, F., Boutin, J., Escorihuela, M.J., Font, J., Reul, N., Gruhier, C., Juglea, S.E., Drinkwater, M.R., Hahne, A., Martín-Neira, M., Mecklenburg, S., 2010. The SMOS mission: new tool for monitoring key elements of the global water cycle. Proc. IEEE 98, 666–687.
Lakhankar, T., Jones, A.S., Combs, C.L., Sengupta, M., Vonder Haar, T.H., Khanbilvardi, R., 2010. Analysis of large scale spatial variability of soil moisture using a geostatistical method. Sensors (Basel) 10, 913–932.
Larson, K.M., Small, E.E., Gutmann, E.D., Bilich, A.L., Braun, J.J., Zavorotny, V.U., 2008. Use of GPS receivers as a soil moisture network for water cycle studies. Geophys. Res. Lett. 35.
Leavesley, G.H., David, O., Garen, D.C., Nrcs-Usda, N., Goodbody, A.G., Lea, J.K., Marron, J.K., Strobel, M., 2010. A Modeling Framework for Improved Agricultural Water-Supply Forecasting. In.
Legates, D.R., Mahmood, R., Levia, D.F., DeLiberty, T.L., Quiring, S.M., Houser, C., Nelson, F.E., 2011. Soil moisture: a central and unifying theme in physical geography. Prog. Phys. Geogr.: Earth Environ. 35, 65–86.
Liu, C., 2023. Optimization of negative sample selection for landslide susceptibility mapping based on machine learning using K-means-KNN algorithm. Earth Sci. Inf. 16, 4131–4152.
Mao, T., Shangguan, W., Li, Q., Li, L., Zhang, Y., Huang, F., Li, J., Liu, W., Zhang, R., 2022. A spatial downscaling method for remote sensing soil moisture based on random Forest considering soil moisture memory and mass conservation. Remote Sens. 14.
Marczewski, W., Slominski, J., Slominska, E., Usowicz, B., Usowicz, J., Romanov, S., Maryskevych, O., Nastula, J., Zawadzki, J., 2010. Strategies for validating and directions for employing SMOS data, in the Cal-Val project SWEX (3275) for wetlands. Hydrol. Earth Syst. Sci. Discuss. 2010, 7007–7057.
McColl, K.A., Vogelzang, J., Konings, A.G., Entekhabi, D., Piles, M., Stoffelen, A., 2014. Extended triple collocation: estimating errors and correlation coefficients with respect to an unknown target. Geophys. Res. Lett. 41, 6229–6236.
Meng, X., Hu, J., Peng, J., Li, J., Leng, G., Ferhatoglu, C., Li, X., Garcia-Garcia, A., Yang, Y., 2024a. Validation and expansion of the soil moisture index for assessing soil moisture dynamics from AMSR2 brightness temperature. Remote Sens. Environ. 303.
Meng, X., Zeng, J., Yang, Y., Zhao, W., Ma, H., Letu, H., Zhu, Q., Liu, Y., Wang, P., Peng, J., 2024b. High-resolution soil moisture mapping through passive microwave remote sensing downscaling. Innovation Geosci. 2, 100105.
Merlin, O., Chehbouni, A., Boulet, G., Kerr, Y., 2006a. Assimilation of disaggregated microwave soil moisture into a hydrologic model using coarse-scale meteorological data. J. Hydrometeorol. 7, 1308–1322.
Merlin, O., Chehbouni, A., Kerr, Y.H., Goodrich, D.C., 2006b. A downscaling method for distributing surface soil moisture within a microwave pixel: application to the monsoon '90 data. Remote Sens. Environ. 101, 379–389.
Min, X., Li, D., Shangguan, Y., Tian, S., Shi, Z., 2023. Characterizing the accuracy of satellite-based products to detect soil moisture at the global scale. Geoderma 432.
Minet, J., Laloy, E., Lambot, S., Vanclooster, M., 2011. Effect of high-resolution spatial soil moisture variability on simulated runoff response using a distributed hydrologic model. Hydrol. Earth Syst. Sci. 15, 1323–1338.
Musiał, J., Dąbrowska-Zielińska, K., Kiryła, W., Oleszczuk, R., Gnatowski, T., Jaszczyński, J., 2016. Derivation and Validation of the High Resolution Satellite Soil Moisture Products: A Case Study of the Biebrza Sentinel-1 Validation Sites. In. Instytut Geodezji i Kartografii, Warszawa.
Nguyen, H.H., Kim, H., Choi, M., 2017. Evaluation of the soil water content using cosmic-ray neutron probe in a heterogeneous monsoon climate-dominated region. Adv. Water Resour. 108, 125–138.
Ojo, E.R., Bullock, P.R., L'Heureux, J., Powers, J., McNairn, H., Pacheco, A., 2015. Calibration and evaluation of a frequency domain reflectometry sensor for real-time soil moisture monitoring. Vadose Zone J. 14.
Osenga, E.C., Vano, J.A., Arnott, J.C., 2021. A community-supported weather and soil moisture monitoring database of the roaring fork catchment of the Colorado River headwaters. Hydrol. Process. 35.
Palecki, M.A., Bell, J.E., 2013. U.S. climate reference network soil moisture observations with triple redundancy: measurement variability. Vadose Zone J. 12.
Park, J., Johnson, J.T., Majurec, N., Niamsuwan, N., Piepmeier, J.R., Mohammed, P.N., Ruf, C.S., Misra, S., Yueh, S.H., Dinardo, S.J., 2011. Airborne L-band radio frequency interference observations from the SMAPVEX08 campaign and associated flights. IEEE Trans. Geosci. Remote Sens. 49, 3359–3370.
Peel, M.C., Finlayson, B.L., McMahon, T.A., 2007. Updated world map of the Koppen-Geiger climate classification. Hydrol. Earth Syst. Sci. 11, 1633–1644.
Peischl, S., Walker, J.P., Rüdiger, C., Ye, N., Kerr, Y.H., Kim, E., Bandara, R., Allahmoradi, M., 2012. The AACES field experiments: SMOS calibration and validation across the Murrumbidgee River catchment. Hydrol. Earth Syst. Sci. 16, 1697–1708.
Peng, J., Loew, A., Merlin, O., Verhoest, N.E.C., 2017. A review of spatial downscaling of satellite remotely sensed soil moisture. Rev. Geophys. 55, 341–366.
Peng, J., Albergel, C., Balenzano, A., Brocca, L., Cartus, O., Cosh, M.H., Crow, W.T., Dabrowska-Zielinska, K., Dadson, S., Davidson, M.W.J., de Rosnay, P., Dorigo, W., Gruber, A., Hagemann, S., Hirschi, M., Kerr, Y.H., Lovergine, F., Mahecha, M.D., Marzahn, P., Mattia, F., Musial, J.P., Preuschmann, S., Reichle, R.H., Satalino, G., Silgram, M., Van Bodegom, P.M., Verhoest, N.E.C., Wagner, W., Walker, J.P., Wegmuller, U., Loew, A., 2021. A roadmap for high-resolution satellite soil moisture applications - confronting product characteristics with user requirements. Remote Sens. Environ. 252.
Peng, C., Zeng, J., Chen, K.-S., Ma, H., Letu, H., Zhang, X., Shi, P., Bi, H., 2025. Spatial representativeness of soil moisture stations and its influential factors at a global scale. IEEE Trans. Geosci. Remote Sens. 63.
Petropoulos, G.P., McCalmont, J.P., 2017. An Operational in Situ Soil Moisture & Soil Temperature Monitoring Network for West Wales. The WSMN Network. SENSORS, UK, p. 17.
Petropoulos, G.P., Ireland, G., Barrett, B., 2015. Surface soil moisture retrievals from remote sensing: current status, products & future trends. Phys. Chem. Earth. A/B/C/ 83-84, 36–56.
Qian, J., Yang, J., Sun, W., Zhao, L., Shi, L., Shi, H., Liao, L., Dang, C., Dou, Q., 2025. Soil organic carbon estimation and transfer framework in agricultural areas based on spatiotemporal constraint strategy combined with active and passive remote sensing. Remote Sens. 17.
Rahmati, M., Balenzano, A., Bechtold, M., Brocca, L., Fluhrer, A., Jagdhuber, T., Karamvasis, K., Mengen, D., Reichle, R.H., Kim, S.B., Taghizadeh-Mehrjardi, R., Walker, J., Zhu, L.J., Montzka, C., 2026. Soil moisture retrieval from Sentinel-1: lessons learned after more than a decade in orbit. Remote Sens. Environ. 333.
Ramo, R., García, M., Rodríguez, D., Chuvieco, E., 2018. A data mining approach for global burned area mapping. Int. J. Appl. Earth Obs. Geoinf. 73, 39–51.
Rubel, F., Kottek, M., 2010. Observed and projected climate shifts 1901-2100 depicted by world maps of the Koppen-Geiger climate classification. Meteorol. Z. 19, 135–141.
Rüdiger, C., Hancock, G., Hemakumara, H.M., Jacobs, B., Kalma, J.D., Martinez, C., Thyer, M., Walker, J.P., Wells, T., Willgoose, G.R., 2007. Goulburn River experimental catchment data set. Water Resour. Res. 43.
Sabaghy, S., Walker, J.P., Renzullo, L.J., Jackson, T.J., 2018. Spatially enhanced passive microwave derived soil moisture: capabilities and opportunities. Remote Sens. Environ. 209, 551–580.
Schaefer, G.L., Cosh, M.H., Jackson, T.J., 2007. The USDA Natural Resources Conservation Service soil climate analysis network (SCAN). J. Atmos. Ocean. Technol. 24, 2073–2077.
Schlenz, F., dall'amico, J.T., Loew, A., Mauser, W., 2012. Uncertainty assessment of the SMOS validation in the upper Danube catchment. IEEE Trans. Geosci. Remote Sens. 50, 1517–1529.
Senanayake, I.P., Pathira Arachchilage, K.R.L., Yeo, I.-Y., Khaki, M., Han, S.-C., Dahlhaus, P.G., 2024. Spatial downscaling of satellite-based soil moisture products using machine learning techniques: a review. Remote Sens. 16.
Smith, A.B., Walker, J.P., Western, A.W., Young, R.I., Ellett, K.M., Pipunic, R.C., Grayson, R.B., Siriwardena, L., Chiew, F.H.S., Richter, H., 2012. The Murrumbidgee soil moisture monitoring network data set. Water Resour. Res. 48.
Su, Z., Wen, J., Dente, L., van der Velde, R., Wang, L., Ma, Y., Yang, K., Hu, Z., 2011. The Tibetan plateau observatory of plateau scale soil moisture and soil temperature (Tibet-Obs) for quantifying uncertainties in coarse resolution satellite and model products. Hydrol. Earth Syst. Sci. 15, 2303–2316.
Tagesson, T., Fensholt, R., Guiro, I., Rasmussen, M.O., Huber, S., Mbow, C., Garcia, M., Horion, S., Sandholt, I., Holm-Rasmussen, B., Gottsche, F.M., Ridler, M.E., Olen, N., Lundegard Olsen, J., Ehammer, A., Madsen, M., Olesen, F.S., Ardo, J., 2015. Ecosystem properties of semiarid savanna grassland in West Africa and its relationship with environmental variability. Glob. Chang. Biol. 21, 250–264.
van der Velde, R., Benninga, H.J.F., Retsios, B., Vermunt, P.C., Salama, M.S., 2023. Twelve years of profile soil moisture and temperature measurements in Twente, the Netherlands. Earth Syst. Sci. Data 15, 1889–1910.
Wang, C., Gu, X., Zhou, X., Yang, J., Yu, T., Tao, Z., Gao, H., Zhan, Y., Wei, X., Li, J., Zhang, L., Li, L., Li, B., Feng, Z., Wang, X., Fu, R., Zheng, X., Wang, C., Sun, Y., Li, B., Dong, W., 2023. Chinese soil moisture observation network and time series data set for high resolution satellite applications. Sci. Data 10.
Wang, P., Zeng, J., Chen, K.-S., Ma, H., Zhang, X., Shi, P., Peng, C., Bi, H., 2024. Global-scale assessment of multiple recently developed/reprocessed remotely sensed soil moisture datasets. IEEE Trans. Geosci. Remote Sens. 62.
Yang, K., Qin, J., Zhao, L., Chen, Y., Tang, W., Han, M., Lazhu, Chen, Z., Lv, N., Ding, B., Wu, H., Lin, C., 2013. A multiscale soil moisture and Freeze–Thaw monitoring network on the third pole. Bull. Am. Meteorol. Soc. 94, 1907–1916.
Yang, G., Guo, P., Li, X., Wan, H., Meng, C., Wang, B., 2020. Assessment with remotely sensed soil moisture products and ground-based observations over three dense network. Earth Sci. Inf. 13, 663–679.
Ye, N., Walker, J.P., Bindlish, R., Chaubell, J., Das, N.N., Gevaert, A.I., Jackson, T.J., Rüdiger, C., 2019. Evaluation of SMAP downscaled brightness temperature using SMAPEx-4/5 airborne observations. Remote Sens. Environ. 221, 363–372.
Ye, N., Walker, J.P., Wu, X., de Jeu, R., Gao, Y., Jackson, T.J., Jonard, F., Kim, E., Merlin, O., Pauwels, V.R.N., Renzullo, L.J., Rudiger, C., Sabaghy, S., von Hebel, C.,

Yueh, S.H., Zhu, L., 2021. The soil moisture active passive experiments: validation of the SMAP products in Australia. IEEE Trans. Geosci. Remote Sens. 59, 2922–2939.
Zhang, D., Zhou, G., 2016. Estimation of soil moisture from optical and thermal remote sensing: a review. Sensors (Basel) 16.
Zhang, P., Zheng, D., van der Velde, R., Wen, J., Zeng, Y., Wang, X., Wang, Z., Chen, J., Su, Z., 2021. Status of the Tibetan plateau observatory (Tibet-Obs) and a 10-year (2009-2019) surface soil moisture dataset. Earth Syst. Sci. Data 13, 3075–3102.
Zhang, Y., Liang, S., Ma, H., He, T., Wang, Q., Li, B., Xu, J., Zhang, G., Liu, X., Xiong, C., 2023. Generation of global 1 km daily soil moisture product from 2000 to 2020using ensemble learning. Earth Syst. Sci. Data 15, 2055–2079.
Zhao, T., Shi, J., Lv, L., Xu, H., Chen, D., Cui, Q., Jackson, T.J., Yan, G., Jia, L., Chen, L., Zhao, K., Zheng, X., Zhao, L., Zheng, C., Ji, D., Xiong, C., Wang, T., Li, R., Pan, J., Wen, J., Yu, C., Zheng, Y., Jiang, L., Chai, L., Lu, H., Yao, P., Ma, J., Lv, H., Wu, J., Zhao, W., Yang, N., Guo, P., Li, Y., Hu, L., Geng, D., Zhang, Z., 2020. Soil moisture experiment in the Luan River supporting new satellite mission opportunities. Remote Sens. Environ. 240.
Zheng, C., Jia, L., Zhao, T., 2023. A 21-year dataset (2000−2020) of gap-free global daily surface soil moisture at 1-km grid resolution. Sci. Data 10.
Zhong, Y., Wei, Z., Miao, L., Wang, Y., Walker, J.P., Colliander, A., 2024. Downscaling passive microwave soil moisture estimates using stand-alone optical remote sensing data. IEEE Trans. Geosci. Remote Sens. 62.
Zhu, Z., Woodcock, C.E., 2012. Object-based cloud and cloud shadow detection in Landsat imagery. Remote Sens. Environ. 118, 83–94.
Zhu, L.J., Si, R., Shen, X.J., Walker, J.P., 2022. An advanced change detection method for time-series soil moisture retrieval from Sentinel-1. Remote Sens. Environ. 279.
Zhu, L.J., Yuan, S.S., Liu, Y., Chen, C., Walker, J.P., 2023. Time series soil moisture retrieval from SAR data: multi-temporal constraints and a global validation. Remote Sens. Environ. 287.
Zhu, L.J., Dai, J.J., Liu, Y., Yuan, S.S., Qin, T.L., Walker, J.P., 2024. A cross-resolution transfer learning approach for soil moisture retrieval from Sentinel-1 using limited training samples. Remote Sens. Environ. 301.
Zhu, L.J., Cai, Q., Jin, J.L., Yuan, S.S., Shen, X.J., Walker, J.P., 2025a. Multi-scale domain adaptation for high-resolution soil moisture retrieval from synthetic aperture radar in data-scarce regions. J. Hydrol. 657.
Zhu, L.J., Dai, J.J., Jin, J.L., Yuan, S.S., Xiong, Z.W., Walker, J.P., 2025b. Are the current expectations for SAR remote sensing of soil moisture using machine learning overoptimistic? IEEE Trans. Geosci. Remote Sens. 63.
Zreda, M., Desilets, D., Ferré, T.P.A., Scott, R.L., 2008. Measuring soil moisture content non-invasively at intermediate spatial scale using cosmic-ray neutrons. Geophys. Res. Lett. 35.